Biomass and Bioenergy 204 (2026) 108401

Contents lists available at ScienceDirect

Biomass and Bioenergy

journal homepage: www.elsevier.com/locate/biombioe

Sustainable biochar production from shrimp pond algal waste: Optimization of pyrolysis parameters using the L9 Taguchi method

Shushree Prachi Palai [a], Soumyaranjan Senapati [a], Sthitiprajna Muduli [b], Alok Kumar Panda [a], Tapan Kumar Bastia [a,*], Pankaj Kumar Parhi [c,**]

[a] Environmental Science Laboratory, School of Applied Sciences, Kalinga Institute of Industrial Technology, Deemed to Be University, Bhubaneswar, 751024, Odisha, India
[b] Department of Chemistry, School of Applied Sciences, Kalinga Institute of Industrial Technology, Deemed to Be University, Bhubaneswar, 751024, Odisha, India
[c] Department of Chemistry, Fakir Mohan (F.M.) University, Vyasa Vihar, Balasore, 756089, Odisha, India

ARTICLE INFO

Keywords:
Algal biochar
Pyrolysis
Taguchi method
Pearson correlation matrix
Characterization techniques

ABSTRACT

Algal blooms *(Spirogyra)*, a common environmental challenge in shrimp farming, offer a valuable opportunity for sustainable waste conversion into biochar. This study evaluates the feasibility of producing biochar from algal biomass through pyrolysis, focusing on optimizing three key process parameters: temperature, residence time, and heating rate. An L9 Taguchi orthogonal array was used to design the experiments. Biochar yield and quality were analyzed using advanced characterization techniques, including PXRD, FESEM, EDAX, CHNS, RAMAN, FTIR, BET, XPS, analysis, particle density, and pH measurement, to understand the physicochemical properties of the resulting biochar. From the characterization data, the optimization of biochar yield in the context of the functional group's perspective and surface area is 70.5 % and 66.1 %, respectively. The pyrolyzed product, pristine biochar, demonstrated that processing conditions significantly influence biochar structure and properties quantitatively and qualitatively. These findings provide insight into optimal pyrolysis parameters for enhancing biochar quality, with potential applications in environmental remediation and agricultural sustainability.

1. Introduction

The Industrial Revolution, driven by scientific and technological advances, triggered major environmental issues like climate change, pollution, and resource depletion. Fossil fuels, meeting 80 % of global energy demand, are the main source of greenhouse gas emissions. To mitigate this, developing renewable energy, adopting carbon capture, and replacing fossil fuels are essential. To overcome the drawbacks of fossil-derived products, biomass-based alternatives—such as fuels, power, and chemicals are gaining traction for their renewability, lower emissions, and sustainability. Biomass now stands out as a viable energy source, helping reduce dependence on non-renewables, which still supply 14 % of global energy annually. Biomass exists in various forms, including animal dung, municipal waste, forest residues, agro waste [1], and aquatic invasive plants. It is categorized by origin into primary (natural), secondary (agricultural waste), tertiary (other by-products) residues [2], and by composition into non-lignocellulosic and lignocellulosic types [3]. With around 2.2×10^{11} tons of lignocellulosic biomass produced annually, its abundance highlights the strong potential of biomass as a renewable energy source.

Algae, a promising aquatic crop, offer thermochemical feedstock potential due to their rapid growth, minimal space needs, and water efficiency [2,3]. Both freshwater and marine macroalgae serve diverse uses and support ecological balance. Their high CO_2 fixation, fast biomass production, and potential to produce valuable compounds like lipids, proteins, pigments, starches make them suitable for energy, food, pharma, wastewater treatment, and pollution control. Recently, waste algal biomass has been used to produce functional biochar via thermochemical processes, reducing costs and environmental impact [4].

Biochar is a carbon-rich, porous material produced by thermochemically decomposing biomass under low or no oxygen conditions [5]. The thermochemical breakdown processes to produce biochar like pyrolysis, hydrothermal carbonization, gasification, torrefaction, and microwave heating vary in temperature and duration [6–8]. Biochar is gaining attention for two key reasons: it stabilizes carbon, reducing greenhouse gas emissions [9], and serves as a low-cost, eco-friendly

* Corresponding author.
** Corresponding author.
E-mail addresses: tapan.bastiafch@kiit.ac.in (T.K. Bastia), parhipankaj@gmail.com (P.K. Parhi).

https://doi.org/10.1016/j.biombioe.2025.108401
Received 19 March 2025; Received in revised form 14 August 2025; Accepted 15 September 2025
Available online 18 September 2025

adsorbent due to its high surface area and functional groups [10–12]. It's widely used for metal adsorption, water purification, soil enhancement, and clean energy production, while also aiding in pollutant removal and emission reduction [13]. These benefits make biochar valuable for tackling soil degradation, pollution, and climate change, while also supporting waste management and sustainable development. Algal biochar, in particular, stands out for its high surface area, hydrophilicity, oxygenated groups, porous structure, and low cost, making it a promising alternative to nanocarbons like graphene and CNTs in applications such as energy storage and environmental remediation [14,15].

Algal biomass is an ideal pyrolysis feedstock due to its unique properties such as the absence of complex polymers (like lignin, cellulose, hemicellulose), low O/C ratio (yielding high calorific value), low ash content, and low energy input requirements [14,16–19]. These traits allow efficient degradation at lower temperatures, enhancing both energy efficiency and biochar quality. Pyrolysis performance depends on factors such as reactor type, feedstock composition, and operating conditions including temperature, heating rate, residence time, gas flow, particle size, and catalysts [20–22]. Proper optimization improves the amount and quality of products, making pyrolysis a very effective way to use algal biomass [23].

Shrimp farming systems especially in intensive or semi-intensive aquaculture (in this case ponds), often experience rapid microalgae growth due to nutrient-rich [24] water. The water in these ponds is high in nitrogen and phosphorus from shrimp feed and [25] excreta. So, the algae biomass from here can contribute to water quality control initially. But these same algae can become problematic when they accumulate excessively or die off, leading to algal blooms, oxygen depletion, and waste management [26,27] challenges. Thus, rather than treating this algal biomass as waste, our study proposes a sustainable utilisation strategy, i.e., converting it into biochar via pyrolysis.

As pyrolysis temperature changes, oxygen-containing functional groups on biochar—especially carboxyl groups undergo significant transformation [14]. For example, marine algae pyrolysis converts cellulose into esters or carboxyl groups, but higher temperatures cause these groups to degrade or carbonize, reducing active sites and heavy metal adsorption capacity [28]. Thus, optimizing pyrolysis temperature is key to retaining oxygen-rich functional groups. Algal biochar, containing both oxygen- and nitrogen-functional groups, shows strong potential for pollutant removal [29,30]. Although its surface area is typically low, it increases with temperature [15]. However, biochar yield declines with rising temperatures, as shown in studies on *Saccharina japonica*, *Sargassum fusiforme* [28], and *Eucheuma spinosum* [31]. At 600–800 °C, pore volume, phosphate sorption, and surface area decline due to pore collapse [32,33]. The thermochemical conversion of algal biomass remains complex, and the combined effects of key pyrolysis parameters like temperature, heating rate and residence time on algal biochar yield and properties are still underexplored. Thus, optimization for high-quality algal biochar production is still a research gap.

This study presents, baseline information that enables the assessment of the primary parameters of pyrolysis on algal biochar, its physicochemical properties, and the optimization of both qualitative and quantitative aspects using the L9 Taguchi method.

The Taguchi methodology is a statistical approach developed by Genichi Taguchi to improve the quality of optimization process parameters with minimal experimental effort. It uses orthogonal arrays and signal-to-noise (S/N) ratio to systematically design experiments, allowing the evaluation of multiple factors and their interactions [34] efficiently, which is why it has been chosen for this study [35]. Its use of orthogonal arrays allows for the systematic evaluation of key variables—such as pyrolysis temperature, heating rate, and residence time—while reducing experimental complexity [36]. This method verifies the interactions between parameters to significantly influence product quality and yield. Moreover, the S/N ratio analysis helps identify the earliest given conditions, ensuring consistent biochar quality under varying operational settings.

2. Experimental

2.1. Materials and methods

To prepare algal bloom (Spirogyra) biochar, biomass was obtained from a shrimp aquaculture farm in Rajkanika, Kendrapara, India. The collected biomass was washed thoroughly with tap water, followed by distilled water multiple times to remove dirt and soil particles. It was then dried under the sun to reduce the moisture content. After drying, the biomass was ground using a Bajaj grinder and sieved to obtain a fine particle size of 0.150 mm, ensuring a uniform texture for optimal pyrolysis. The finely processed biomass was then subjected to pyrolysis in a Tubular furnace under oxygen-free conditions. The pyrolysis was conducted at three different temperatures—650 °C, 550 °C, and 450°C—with varying residence times of 60, 90, and 120 min. In addition, three different heating rates were applied: 5 °C/min, 10 °C/min, and 15 °C/min. The material produced from this pyrolysis process is referred to as pristine biochar, and its properties were influenced by variations in temperature, pH, and heating rate—key factors in determining its suitability.

2.2. Experimental design and statistical implementation

In this current study Taguchi L9 OA design of experiment (DOE) has been implemented to design the experimental strategy. Three operational parameters, referred to as control factors, are used in this study's L9 orthogonal array: the pyrolysis temperature (°C), residence time (min), and heating rate(°C/min), each of which has three levels, as indicated in Table 1. The L9 Taguchi orthogonal array experiments were designed using MINITAB 14. Table 2, shows a maximum of 9 combinations of three operational parameters for the experimental setup by using the L9 Taguchi orthogonal array. By considering the mean value, variance, and signal-to-noise (S/N) ratio, Taguchi design assesses pairs of combinations to identify the optimal levels that contribute to the optimum response value [37]. To ensure robust optimization, both "larger-is-better" and "smaller-is-better" criteria were considered, depending on the nature of the desired output and demonstrated in Eqs. [1,2], respectively.

Larger-is-Better (used when the goal is to maximize the response, e.g., biochar yield):

$$S/N = -10\log_{10}\left(\frac{1}{n}\sum_{i=1}^{n}\frac{1}{y_i^2}\right) \quad [1]$$

Smaller-is-Better (used when the goal is to minimize the response, e.g., impurities or emissions):

$$S/N = -10\log_{10}\left(\frac{1}{n}\sum_{i=1}^{n}y_i^2\right) \quad [2]$$

Here.

- n = number of repetitions for a given trial
- y_i = observed response value for the i-th repetition

Where n is the number of repetitions for a given trial, and yi is the

Table −1
Taguchi L9 orthogonal array design of experiments.

Parameter	Level 1	Level 2	Level 3
Temperature (°C)	450	550	650
Heating rate (°C/min)	5	10	15
Residence time (Min)	60	90	120

Table −2
PYROLYSIS of biomass Taguchi L9 orthogonal array design of EXPERIMENTS ✓ **design of experiments (3 factors * 3LEVELS).**

Run	ALGAL Material name	Temperature (°C)	Heating rate (°C/min)	Residence time (Min)
1	**A1**	**450**	**5**	**60**
2	**A2**	**550**	**10**	**90**
3	**A3**	**650**	**15**	**120**
4	**A4**	**450**	**10**	**120**
5	**A5**	**550**	**15**	**60**
6	**A6**	**650**	**5**	**90**
7	**A7**	**450**	**15**	**90**
8	**A8**	**550**	**5**	**120**
9	**A9**	**650**	**10**	**60**

observed response value. A higher S/N ratio indicates improved performance and reduced variability. Level-wise S/N means were computed, followed by Δ (max–min) and ranking to identify the most influential factors. The delta value, calculated as the difference between the maximum and minimum mean S/N ratios for each factor, was used to rank factor significance as demonstrated in Equation [3]. Main effect and interaction plots were generated to visually interpret the effect of each factor and its combinations on the response. The optimal factor setting was identified by selecting the level with the highest S/N ratio for each factor [38,39].

$$\Delta_j = \max\left(\overline{S/N_j}\right) - \min\left(\overline{S/N_j}\right) \quad [3]$$

where $\overline{S/N_j}$ represents the average S/N ratio at each level of the factor *j*. The factor with the highest delta value was considered the most influential on biochar yield.

2.3. Pearson correlation matrix

Pearson correlation analysis was conducted to quantify the strength and direction of the linear relationship between process parameters—temperature, residence time, and heating rate—and biochar properties, including yield, H/C ratio, O/C ratio, surface area, and particle density. The correlation coefficient (r) was calculated using Equation [4].

$$r = \frac{\sum (X_i - \overline{X})(Y_i - \overline{Y})}{\sqrt{\sum (X_i - \overline{X})^2 \sum (Y_i - \overline{Y})^2}} \quad [4]$$

Where Xi and Yi represent the observed values of the two variables, and $\overline{X}$ and $\overline{Y}$ are their respective means. The Pearson correlation coefficient, denoted as r, ranges from −1 to +1, where the sign indicates the direction of the relationship and the absolute value reflects its strength. A positive r value signifies a direct relationship, meaning both variables tend to increase or decrease together. Conversely, a negative r value indicates an inverse relationship, where an increase in one variable corresponds to a decrease in the other. The closer the 'r' value is to either +1 or −1, the stronger the correlation between the variables, while values near zero suggest a weak or no linear relationship [40].

2.4. Preparation of biochar

Pyrolysis of algal biomass was performed in the tubular furnace (model Ants), and the furnace was maintained in the absence of Oxygen. The nine sets of experiments were run in the furnace with a designed set of temperatures, heating rate, and residence time. The nine biochars obtained were kept in an oven at 100 °C for 4 h. The yield percentage of produced biochar was determined using the following formula in Eqs [5]: where W_1 represents the initial weight of the biomass, and W_2 denotes the weight of the resulting biochar.

$$\text{Biochar Yield (\%)} = (\text{Weight of produced biochar} / \text{Weight of initial biomass}) \times 100 \quad [5]$$

2.4.1. Particle density determination

To find out the density of the particle the following formula(equation:6 &7) has been used.

M_0: Weight of Empty Pycnometer.
M_S: Weight of Solid.
M_1: Weight of solid and pycnometer (M_0+M_S)
M_2: Weight of water and pycnometer (M_0+M_{H2O})
M_3: Weight of solid and water and pycnometer (M_0+M_S + M_{H2O})

$$[M_S = M_1 - M_0]$$

$$[M_{H2O} = M_2 - M_0]$$

$$\left[M'_{H2O} = M_3 - M_1\right]$$

$$V_S = \frac{M_{H2O} - M'_{H2O}}{\rho_{H2O}} \quad [6]$$

$$\rho_S = \frac{M_S}{V_S} \quad [7]$$

2.5. Instrumentation

The elemental composition and surface structure of the biomass and biochar materials were examined using a CHNS analyzer (Thermo Fischer Flash EA 1112), a scanning electron microscope, and an energy-dispersive X-ray (EDAX) (Zeiss Gemini SEM 450). A surface area analyzer (Bellsorp maxi, Microtrac bell crop) using the nitrogen adsorption-desorption method was used to examine the surface area and the pore structure of the material. The functional groups were analyzed using Fourier transform infrared spectroscopy (Thermo-Nicolet), Raman spectroscopy (Renishaw Invia), and X-ray photoelectron spectroscopy (Axis Supra, Kratos Analytical Limited). The Bruker D8 Advance X-ray diffraction spectrometer was used to examine the degree of graphitization. The composition of the hemicellulose, cellulose, and lignin in the biochar and Particle density were measured by pycnometer, (ASTM-D854-14 standard).

3. Results and discussion

3.1. Effect of processing condition on biochar yield and physiochemical properties

The L9 Taguchi orthogonal array, employing temperature, heating rate, and residence time as primary variables, revealed distinct trends in algal biochar yield and properties. A consistent decrease in yield was observed as the pyrolysis temperature increased from 450 °C to 650 °C. This reduction aligns with earlier reports where higher pyrolysis temperatures promoted extensive devolatilization and thermal cracking, thereby reducing solid residue and increasing ash content [41,42]. At 650 °C, the yield reduction was more pronounced than at 450 °C or 550 °C, suggesting near-complete decomposition of volatile matter and enhanced secondary reactions, which is typical for biomass rich in hemicellulose and cellulose [43]. For heating rate, the lowest rate (5 °C/min) yielded less biochar compared to intermediate and higher rates. This finding contrasts with studies on lignocellulosic biomass where slower heating often increases yield [44], possibly due to the different thermal degradation behaviour of algal biomass, which contains more proteins, lipids, and mineral matter. In our case, faster heating may have shortened the exposure time of volatile intermediates to the hot zone, thereby reducing secondary char oxidation.

Residence time also exerted a notable influence: moderate residence

times optimised yield and key physicochemical characteristics such as particle density, BET surface area, and the abundance of carbonyl groups. Excessively short residence times may not allow complete carbonization, while excessively long durations can lead to further gasification and degradation of fixed carbon, as reported in similar studies [45]. Overall, temperature exerted the greatest influence on yield, followed by effects on the C/H ratio, particle density, and surface chemistry. This is consistent with reports that temperature is the dominant factor shaping both the structural order and functional group distribution in biochars [46]. The trends observed in our study thus support the conclusion that optimizing pyrolysis conditions—particularly maintaining moderate residence times and intermediate heating rates while controlling temperature—is critical for balancing yield with desirable physicochemical properties for environmental applications.

3.2. Effect of temperature

The pyrolysis temperature is a critical input parameter in the thermochemical conversion of biomass. A variation in pyrolysis temperature influences the degree of carbonization in biochar, thereby affecting several physicochemical parameters such as yield, pH, pore volume, porosity, surface area carbon content, surface functionality, and hydrophobicity. Higher pyrolysis temperatures produce biochar with higher specific surface area, pH and mineral content, Zeta potential pore volume, aromaticity, fixed carbon content, and persistent free radical (PFR), but lower yield, volatile matter release, surface functionality, sulfur, hydrogen, oxygen, nitrogen, polarity and cation exchange capacity. Conversely, a lower pyrolysis temperature setting produces more char, encourages the buildup of surface functional groups, improves cation exchange capacity, decreases specific surface area, increases water holding capacity, and lowers the char's pH level [47]. According to Lian et al. (2020) [48], the final yield of biochar for invasive horseweed plants decreases from 35.5 to 30.1 % and for ragweed, it decreases from 37.2 to 29.6 % when the pyrolysis temperature increases from 350 °C to 550 °C. Another study found a similar pattern, with the production of biochar reducing from 46.59 to 28.20 % when the Water Hyacinth's pyrolysis temperature raised from 300°C to 700 °C. Three macroalgae (*Porphyra tenera, Lamalia japonica,* and *Undaria pinnatifida*) were pyrolyzed at different temperatures (300–600 °C) in a slow pyrolysis study [49].

The resulting products showed varying yield values and compositions due to the physicochemical characteristics of each macroalga, which included differences in AC (10.44–28.28 wt%), H/C ratio (1.37–192), and O/C ratio (0.88–1.53). According to other studies, the overall behaviors for all macro-algae were decreasing the generation of biochar and rising yields of syngas and bio-oil as the pyrolysis temperatures were increased. *Laminaria japonica*, for example, was carbonized via gradual pyrolysis at 300°C-600 °C before being combined with an alginate solution to maximize and create Ca-alginate beads for phosphate removal [33].

Biochar yields decreased from 78.34 to 27.05 % as the temperature went up, but AC yields increased from 22.92 to 64.19 %. This was mainly caused by the raw algae's alkaline mineral content [3]. Likewise, from this study, we found that when varying temperatures from 450 °C to 650 °C, the biochar yield decreases from 71.75 % to 63 % as temperature increases. Out of 9 sets of experimental combinations, two main temperatures are 450 °C & 550 °C, further selected by confirming their yield in percentage and taking both C/H ratio and C/O ratio values.

3.3. Heating rate

In the pyrolysis of biomass, the heating rate is crucial since it influences the end product's content and character. A low heating rate increases the amount of biochar by preventing the thermal cracking of biomass and lowering the possibility of subsequent pyrolysis processes. A rapid heating rate enhances the potential of biomass disintegration into gas and prevents the repolymerization of algal lipid vapors, even at low temperatures, hence increasing bio-oil production [50]. The low heating rate favors the secondary reaction between a char particle and volatiles to form secondary char while also gently removing the volatile materials [51].

A higher yield of biochar was found in another study when Solidago canadensis biomass was pyrolyzed at 300 °C with a heating rate ranging from 4°C to 8 °C. Low residence time for the gradual degradation throughout the conversion process, which results in reactions favoring the polymerization of cellulose, may be the cause of the increased biochar production [12]. From Fig. 1. Our chosen set of heating rates is, 5, 10,15 °C/min with respect to temperature and residence time. From Fig. 1, we observed that at 450 °C, while varying the heating rate from 5, 10,15 °C/min it shows the biochar yield was 70.05 %, 69.65 %, 70.5 %, respectively, showing an irregular pattern. In the case of 550 °C temperature, while increasing in heating rates, biochar yield increased from 62.9 % to 71.75, whereas at 650 °C temperature, at three heating rates average yield is 63 %.

3.4. Feedstock type

Algal biomass (macroalgae and microalgae) possesses a unique composition in contrast to lignocellulosic biomass. Algae are mostly made up of complex, multidimensional organic materials with a unique fibrous structure, including proteins, lipids, and carbohydrates. Furthermore, the chemical composition of algae usually varies among different species and is influenced by various factors, including growth conditions and cultivation techniques. The chemical content and structure of the feedstock can influence the product composition and yield during the pyrolysis process.

Algal biomasses exhibit significant variability in terms of protein, lipid, and carbohydrate content, resulting in the production of products with diverse compositions. Research indicates that the pyrolysis behavior of algal biomass significantly differs from that of lignocellulosic biomass. The carbohydrates, proteins, and lipids in algal biomass can be pyrolyzed more readily than the primary constituents of lignocellulosic biomass, particularly those with elevated lignin content, resulting in a greater bio-oil yield [22]. Biochar yields decrease with rising pyrolysis temperatures. The pyrolysis algal biochar mostly consists of carbon, hydrogen, nitrogen, ash, and a high percentage of inorganic elements (P, K, Na, Ca, and Mg). The quantity of char produced by algal pyrolysis is significantly more than that obtained from terrestrial biomass sources, attributable to the elevated quantities of ash and fixed carbon found in algal species. The ultimate analysis of biochar formed from microalgae, macroalgae, and lignocellulosic biomass indicates that

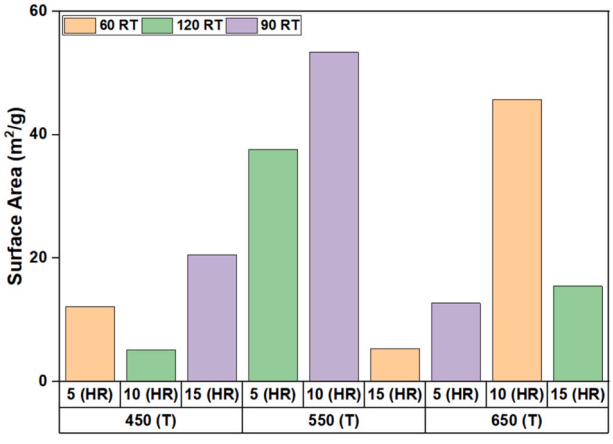

Fig. 1. Bar diagram showing the surface area from BET analysis of 9 set of algal biochar with respect to Temperature, Heating rate, Residence Time.

the properties of pyrolysis-derived biochars from microalgae are comparable to those from macroalgae, but distinct from those of lignocellulosic biomass.

Algal biochars possess a reduced carbon concentration compared to lignocellulosic biochar, though they indicate higher pH, nitrogen levels, ash content, and inorganic components [52]. The initial and essential step in assessing the utility and applications of algal biochar involves quantifying its properties and comparing them with biochar derived from other widely utilized terrestrial biomass feedstocks. Current studies indicate that biochars derived from algal samples exhibit fundamental differences compared to those generated from lignocellulosic feedstock. Typically, biochars derived from different algal species exhibit low levels of carbon content, surface area, and cation exchange capacity, while showing elevated pH, nitrogen, and extractable inorganic nutrients such as phosphorus, potassium, calcium, and magnesium. In contrast, biochars derived from lignocellulosic materials typically exhibit higher carbon contents and enhanced cation exchange capacities, with pH values generally below 7, with specifically reduced ash and available nutrient levels [53].

3.5. Characterization

3.5.1. BET

From Fig. 2 and Table 3, it is revealed that when the temperature increased from 450 °C to 650 °C surface area of algal biochar increased to 53.382 m^2/g maximum out of 9 pyrolysis experimental setups. Out of three residence times, 90 min showed comparatively higher surface area than the 60 min & 120 min, whereas at 450 °C temperature with residence time of 120min showed 5.120 m^2/g from the BET data. From the above data, it is confirmed that pyrolysis temperature and residence time have a significant influence on the surface area of algal biochar than the heating rates.

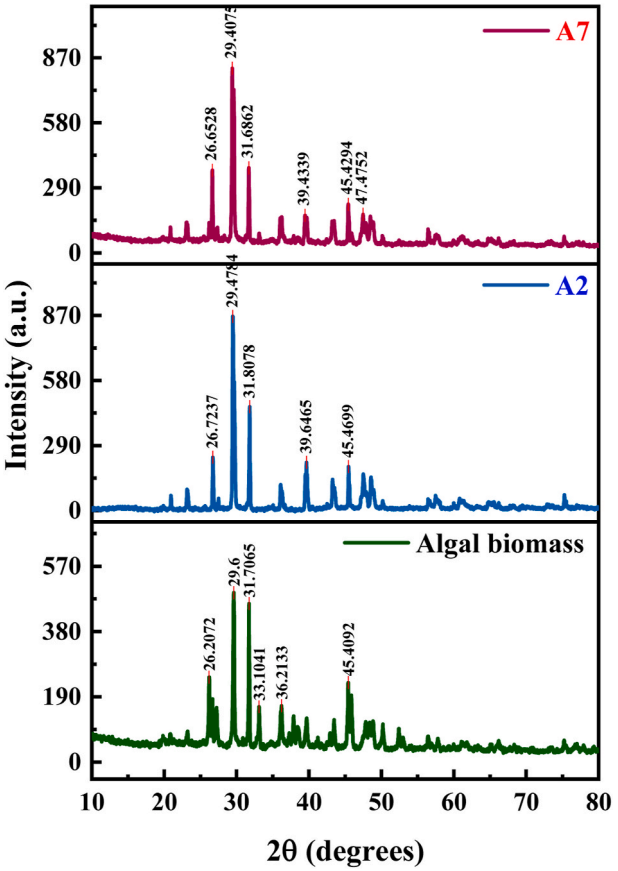

Fig. 2. PXRD graphs of Algal biomass, A2 biochar, A7 biochar.

With an increase in pyrolysis temperature, a greater release of volatile compounds occurs from the algal biomass, resulting in a more porous structure that creates a wider surface area [54]. Higher surface area can also result from faster pyrolysis heating rates because pores form rapidly [55]. The duration of "residence time" during pyrolysis plays a crucial role in influencing surface area. A longer presence of algal biomass in the pyrolysis reactor allows for greater pore development and an increase in overall surface area. However, it is important to note that excessively prolonged residence times may result in pore collapse, ultimately diminishing the surface area once more [56], whereas shorter residence times fail to create a porous structure and a lack of heat transfer in the cell resulted in lower surface area. The BET surface area of the sample showed a general enhancement with the increase in pyrolysis temperature. The experimental results and the characteristics of the pyrolytic products aligned with observations from other studies on macroalgae, including Saccharina japonica [57]. Nevertheless, biochar derived from macroalgae exhibits a comparatively greater surface area (reaching up to 80 m^2/g), which can be essential for applications in catalysis and wastewater treatment [3,58]. Investigated biochar obtained from macroalgae and found that the biochar from Eucheuma sp. exhibited a notably higher surface area, measuring between 30.03 and 34.82 m^2/g, compared to other species, which had surface areas ranging from 1.29 to 8.87 m^2/g.

From the above data, it is confirmed that pyrolysis temperature and residence time have a significant influence on the surface area of algal biochar than the heating rates. A similar kind of result was obtained by Neonjyoti Bordoloi and their group. They found the variation in surface area ranging from 1.72 to 123 m^2/g as pyrolyzing microalgae *Scenedesmus dimorphus* at different temperatures ranging from 300 °C to 600 °C with a heating rate of 40 °C/min [59]. In another study, Ronsse et al. characterized the biochar produced from different feedstock and obtained a variation in surface area with the range of 14–19 m^2/g by pyrolyzing dried algae biomass with a heating rate of 17 °C/min, residence time of 10 and 60 min, and pyrolysis ranging temperature between 300 °C and 750 °C [60].

3.5.2. PXRD

Patterns for algal biomass and biochars at 450 °C, 550 °C, and 650 °C are illustrated in Fig. 2 & Fig. S2. Due to the presence of minerals in the samples, two forms of crystalline structure were discovered after all the samples exhibited highly similar XRD signals. These were halite at 2θ = 31°–32°∘ and 45°–46°, and sylvite at 2θ = 28°–29°, 40°–41°, 50°–51°, 56°–58°. Crystals of KCl and NaCl are represented by sylvite and halite, respectively. As the temperature of pyrolysis increased, the strength of the peaks shifted because the biomass structure was destroyed [61], which was in agreement with the standard graphite's XRD patterns. The diffraction peaks observed at various line counts corresponding to 2θ = 30°, 32°, 40°, and 45° illustrate the crystalline structures present in the cellulose of the biochar sample. Fig. 2 and Fig. S2 indicate that the broadening reveals the alignment of crystallites in relation to the aromatic layers, with the peaks observed at 2θ = 20°–30° corresponding to the structural arrangement of the aromatic layers (graphite 002). The presence of sharp, unidentified peaks in biochar indicates the presence of several inorganic components. The increased occurrence of these peaks aligns with the elevated levels of SiO_2, CaO, and MgO, though this aspect has not been thoroughly explored. The crystalline SiO_2 accounts for the significant and primary peak observed at 2θ = 29°. The X-ray diffraction peak indicated that the biochar surface exhibits heterogeneity [62]. The most significant of them were crystalline quartz (SiO_2) and calcite ($CaCO_3$), while other intense peaks were associated with alkaline and alkaline salts.

As the temperature increases in conjunction with the heating rate, many peaks become collapsed and more intensified, resulting in sharper peaks. However, a 90-min residence time shows better, sharper, and more stable peaks compared to other residence times, likely due to the complete decomposition of cellulose materials in the algal biochar.

Table 3
Input variables and output responses of 9 set of algal biochar.

Exp No.	ALGAL Material name	INPUT VARIABLES			OUTPUT RESPONSES			
		Pyrolysis Temperature (°C)	Heating rate (°C/min)	Residence time (Min)	Yield (%)	(H/C)	(O/C) EDX	SA
1	**A1**	450	5	60	70.05	0.066	1.746	12.164
2	**A2**	550	10	90	66.1	0.036	2.481	53.382
3	**A3**	650	15	120	59.65	0.012	1.618	15.460
4	**A4**	450	10	120	69.65	0.078	1.689	5.120
5	**A5**	550	15	60	71.75	0.126	1.751	5.320
6	**A6**	650	5	90	63.85	0.088	1.968	12.710
7	**A7**	450	15	90	70.5	0.120	2.760	20.548
8	**A8**	550	5	120	62.9	0.061	2.737	37.657
9	**A9**	650	10	60	63	0.028	1.916	45.747

Furthermore, the prominent and distinct XRD reflection peaks confirmed that the synthesized material exhibited excellent crystallinity.

3.5.3. *FESEM & EDAX*

From Fig. 3 and Fig. S5 FESEM images reveal that while algal biomass primarily exhibits a spherical morphology, biochar undergoes deformation due to cell fragmentation during lipid extraction [63]. Wang et al., 2017 reported a compact, irregular and heterogeneous surface. The FESEM analysis further indicates that as the temperature increases from 450 °C to 650 °C, surface pores tend to melt and collapse. Additionally, the images confirm the deposition of minerals and inorganic salts, appearing as fiber-like structures. The FESEM images presented indicate that higher heating treatment of Spirogyra may yield a more uniform structure, whereas the lower heating process appears to result in blocks exhibiting irregular and shattered morphology [64].

3.5.4. *FTIR spectroscopy*

Fourier transform infrared (FTIR) spectroscopy was used within the range of 400–4000 cm^{-1} to study the influence of pyrolysis and heating rate on the generation of functional groups on the surface of the biochar. The existence of these functional groups determines the surface reactivity of the biochar. Fig. 4 & S1 and Table 4 show the functional groups

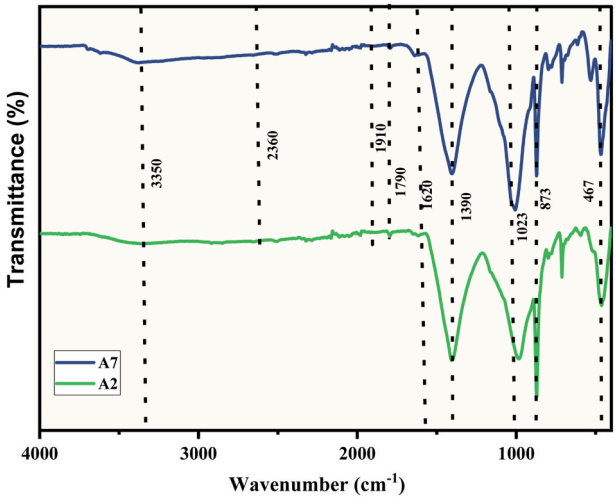

Fig. 4. FTIR graph of A2, A7 Algal biochar.

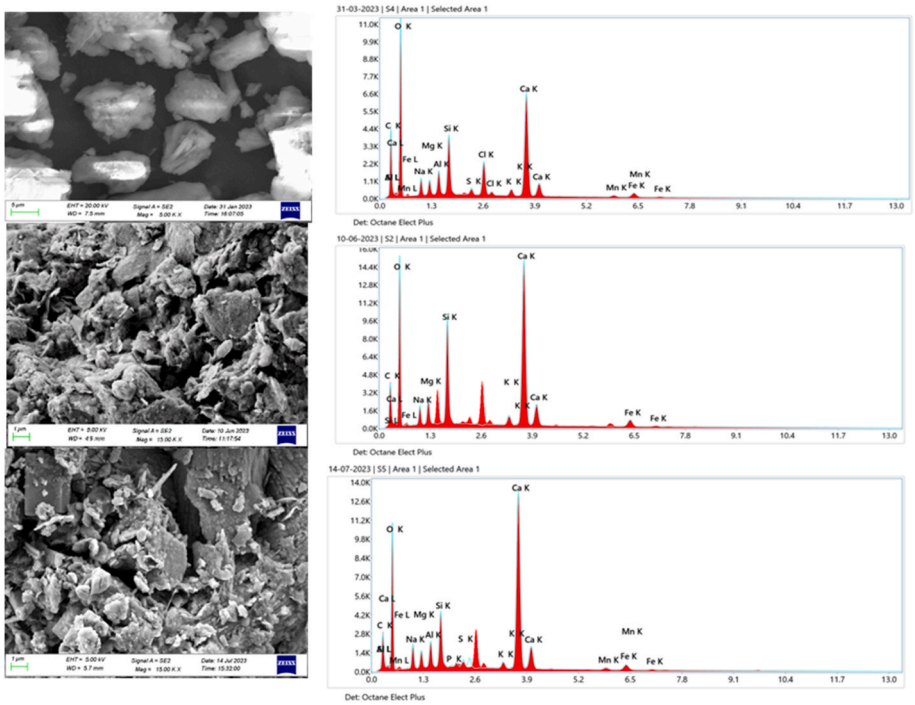

Fig. 3. FESEM images of Algal (Spirogyra) biomass, A2 algal biochar, A7 algal biochar (From top to bottom).

Table 4
FTIR peaks of A2, A7 algal biochar.

Wavenumber (cm^{-1})	Functional groups	References
3350	-OH (Stretching)	[31]
1910–2360	-C=O (Stretching, Ketene)	[59,64]
1730–1150	Heteroatom functional groups	[64]
1617–1635	-C=O stretching (aromatic ring)	[11]
1390	Aliphatic C−H stretching	[11]
1023	Primary alcohols and carbohydrates (C−O stretching)	[11]
873	Polycyclic aromatic hydrocarbons (PAHs)	[23]
467	Si-O-Si (Bending)	[48,66]

present in the algae biomass-derived biochar. All biochar samples show an important hydroxyl group (-OH) stretching vibration peak at about 3350 cm^{-1} [65]. High temperatures of pyrolysis lead to a decrease in the O-H stretching may be due to dehydration (Fig. S1) [51,53]. The stretching of the carbonyl bond (-C = O) in ketene is seen as crests within the range of approximately 1910–2360 cm^{-1} (Fig. 4 and Fig. S1) [66, 67]. The peaks in the range of 1617–1635 cm^{-1} and ~1790 cm^{-1} may be due to the stretching of C=O aromatic rings [68,69]. Similarly, a peak at 1390 cm^{-1} indicates the aliphatic C-H group stretching [68]. The FTIR peaks at 1023 cm^{-1} are present due to the C-O bond stretching of 1° alcohols and carbohydrates [68]. Additionally, peaks at 873 cm^{-1} are located, which may be associated with the presence of polycyclic aromatic hydrocarbons (PAHs) [70]. The FTIR peaks at ~467 cm^{-1} due to the bending vibration of the Si-O-Si bond [71,72]. The trace amounts of silicon in the biochar could be the cause of the silicon bonding. The FTIR spectra show that the surface of the biochar is reached in oxygen-containing functional groups. As a general conclusion from the FTIR analysis, it can be stated that the number of functional groups is less at the high pyrolysis temperature, i.e., 650 °C (Fig. S1C). The presence of more functional groups with greater oxygen-containing functional groups at low pyrolysis temperatures of the biochar helps in adsorbing the pollutant-containing wastewater.

3.5.5. Raman analysis

Raman spectroscopy was used to determine the degree of graphitization of biochar [73]. The analysis of biochar using Raman spectroscopy suggested the presence of G and D bands at ~1598 and ~1350 cm^{-1}, respectively (Fig. 5 and Fig. S3) [73]. The G-band, which lies between 1580 and 1605 cm^{-1}, corresponds to in-plane bond-stretching movements of groups of sp^2 carbon atoms in small chains and rings, signifying the presence of graphitic carbon [68]. Similarly, the D-band, positioned between 1334 and 1361 cm^{-1}, is associated with carbon atoms that have defects or disordered structures, commonly found in amorphous biochar. The I_D/I_G ratio indicates the extent of the disorder and structural organisation of the biochar [68]. The Raman spectra of all the algae biochar ranged from 800 to 1800 cm^{-1} and have been curve-fitted with two bands, namely D and G bands (Fig. 5 and Fig. S3). As the pyrolysis temperature increases, from 450 °C to 650 °C, there are more defects in the biochar structure with I_D/I_G values ranging from 2.23 to 2.83 (Fig. 5 and Fig. S3). This indicates that a greater number of aromatic rings with graphitic structure may be present at the lower pyrolysis of algae biochar. This helps in increasing the π – π interaction between the adsorbent algae biochar and the adsorbate pollutant [74].

3.5.6. XPS analysis

X-ray photoelectron spectroscopy (XPS) analysis was used to determine the elemental composition, oxidation states, chemical bonding, and functional groups of the biochar [75,76]. The surface containing functional groups and the deconvoluted spectra of C1s, N1s, and O1s of the algae biochar (A2 and A7) are shown in Fig. 6 and Table S1. The deconvolution spectra of C1s of the algae biochar show 3 types of peaks. The graphitic and aromatic network peak is due to the C-C and C=C at 284.5eV and 285.5eV due to the C-OH of alcoholic and phenolic groups shown in both of the algae biochar materials (Fig. 6 and Table S1) [75, 77–79]. The peak at 285.7eV due to the C-N amine groups is only present in the A7 algae biochar (Fig. 6 and Table S1) [75]. Similarly, N1s deconvoluted shows two types of common peaks at 399.4eV/400eV are present on both of the algae biochar, presenting the amine group (Fig. 6 and Table S1) [75,80,81]. The O1s deconvoluted spectra show 4 different types of peaks for both of the algae biochar, with peaks at 531.4eV, 532.3eV, and 532.8eV common on both of the biochar, presenting carbonyl/carboxyl, hydroxyl, and phenolic/ether bonded groups respectively (Fig. 6 and Table S1) [76,82–84]. The peak at 533.1eV is present in only A7 algae biochar, and this presents the ester, anhydride, and aromatic C=O groups (Fig. 6 and Table S1) [82,85]. So, from the XPS analysis, it is confirmed that both the A2 and A7 algae biochar contain carbon and oxygen functional groups of the surface biochar with richer oxygen-containing groups (with O/C for A2 = 0.72 and A7 = 0.34), and that helps in adsorbing the wastewater containing pollutants by enhancing the surface hydrophilicity nature of the biocarbon [86]. Also, from the EDX elemental analysis data, the O/C ratio is highest for both the A2 and A7 biochar (i.e., A2 = 2.481 and A7 = 2.760) as compared to other algae biochar material, which enhances the XPS analysis data and indicates both are richer in oxygen functionalities [84, 86].

Also, from the EDX elemental analysis data, the O/C ratio is highest for both the A2 and A7 biochar (i.e., A2 = 2.481 and A7 = 2.760) as compared to other algae biochar material, which enhances the XPS analysis data and indicates both are richer in oxygen functionalities [84, 86]. The additional lower-intensity XPS peaks are identified at around 100eV–102eV, 150eV–152eV, 340eV–360eV, and 1070eV–1072eV, corresponding to Si-2p, Si-2s, Ca-2p, and Na-1s, respectively (Fig. S6). This result is in line with the result obtained from the characterization of EDAX and XRD, which shows that an appreciable amount of silicon,

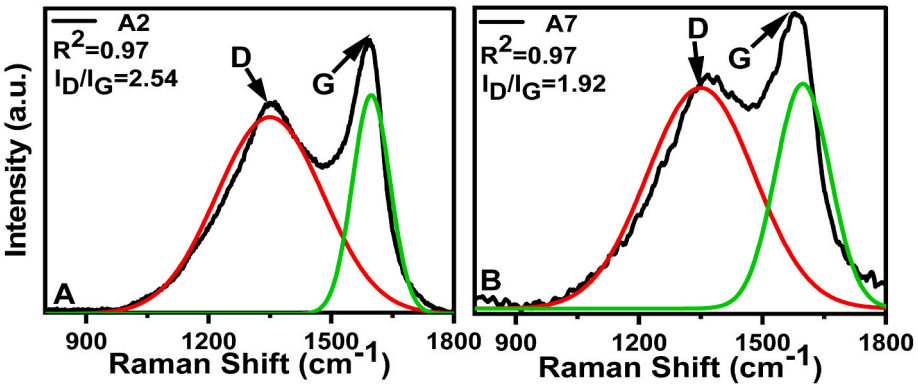

Fig. 5. Raman spectra of algae biochar (A) A2, (B) A7.

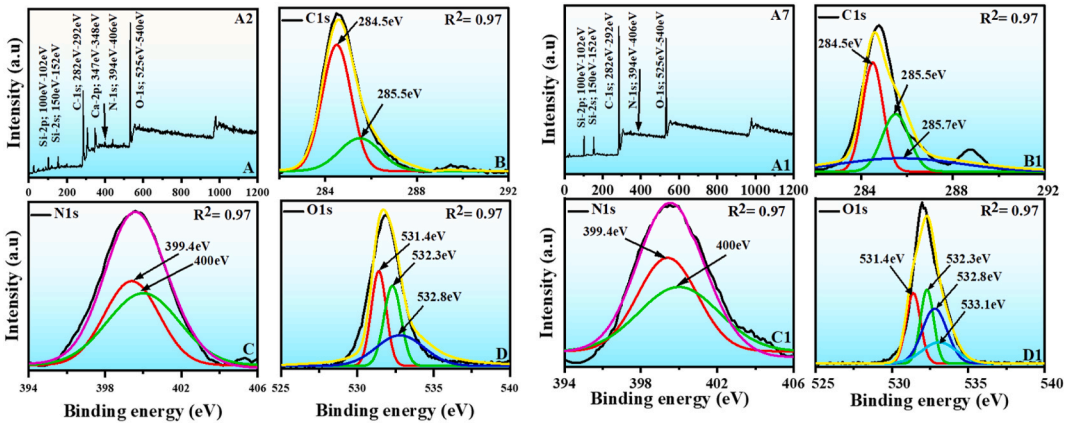

Fig. 6. High-resolution XPS spectra of A2 [(A) full-spectrum, (B) C1s, (C) N1s and (D) O1s], and A7 [(A) full-spectrum, (B) Cs, (C) Ns and (D) Os].

calcium, and sodium is present in both A2 and A7 biochar.

3.5.7. Particle density

According to the particle density analysis of algal biochar using a pycnometer (ASTM- D854-14 standard), the particle density of biochar generally increases as the pyrolysis temperature increases. As shown in Fig. 7, a higher heating rate frequently results in a slightly higher particle density because the volatile matter decomposes faster, creating a denser char structure. Consequently, the temperature and heating rate generally increase as the biochar particle becomes denser and finer. The shrinking and fracturing of larger particles into small, regular particles caused by pyrolysis led to a decrease in particle size while increasing the actual density of the homogenous species products [87]. It is reported that a qualitative range of particle density is 1.5–2.0 g/cm^{3,} but here particle density is higher due to being rich in silica and inorganic contents (Ca, K, Mg, Na), which is confirmed from of PXRD & EDAX characterizations. [88]. The mechanical stability, rigidity, and feedstock composition are critical factors in the production of biochar, as they greatly affect its final properties such as porosity, density, and particle size. Porosity exhibits an inverse correlation with mechanical stability while showing a direct proportionality to density. A higher particle density of biochar suggests an increased presence of micropores, as these have diameters less than 2 nm. Conversely, if the pyrolysis process results in the formation of more mesopores, which range from 2 to 10 nm in diameter, the particle density of the biochar will decrease [89].

3.5.8. Proximate analysis

The results of proximate analysis of the macroalgae *Spirogyra* biomass and biochar are presented in Table 5. The initial content of volatile matter (VM), ash content (AC), and fixed carbon (FC) content of the selected algae biomass are found to be 40.12 ± 0.41 %, 52.24 ± 0.67 %, and 7.64 ± 0.39 %, respectively. After pyrolysis treatment, both VM and FC decreased, while ash content increased, indicating the thermal degradation of organic components and the concentration effect of the inorganic residues in the biochar [90].

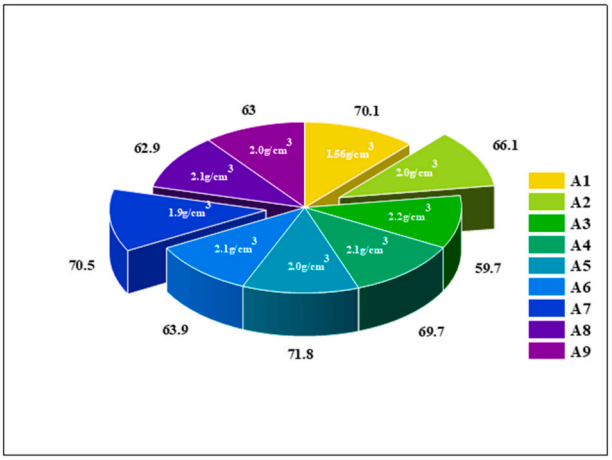

Fig. 7. Pie chart showing particle density and yield% of 9 set of Algal biochar.

3.5.9. pH analysis

Table 6 illustrates that all algal biochars exhibited alkaline properties. The pH of biochar derived from an algal bloom varies between 8.70 and 9.51. When the pyrolysis temperature increases from 450 to 650 °C and the residence time also equal influence as pH decreases when it comes to 120min. The pyrolysis temperature and the algal samples influence the pH of biochar. The study conducted by Ref. [91] indicates a correlation between the pH of biochar and the presence of oxygen functionalities within it [92] found that as the pyrolysis temperature increased from 250 °C to 600 °C, the algal biochar's pH increased from 8.7 to 13.7. The pH behaviour indicates that higher pyrolysis temperatures generally result in algal biochar exhibiting a higher pH. This phenomenon is attributed to the greater presence of alkaline mineral components, such as calcium and potassium, which are released during the decomposition of algal biomass. At lower temperatures (200°C-300 °C), cellulose undergoes decomposition, resulting in the formation of phenolic substances and organic acids. At temperatures exceeding 300 °C, alkali salts separate from organic matter, resulting in an increase in pH [93].

4. S/N analysis

4.1. Result for SA

The Main Effects Plot for Surface Area (SA) reveals that pyrolysis temperature, heating rate, and residence time each have a significant impact on biochar's surface area (Fig. 8(a)). The SA increases from 450 °C to 550 °C and then declines at 650 °C, indicating that 550 °C is the optimal temperature for effective pore development, while higher temperatures may cause pore collapse due to over-carbonization. Similarly, the heating rate of 10 °C/min yields the highest SA, suggesting that moderate heating allows controlled volatile release and better pore structure, whereas a higher rate (15 °C/min) likely causes structural damage. For residence time, 90 min proves to be optimal, as it provides sufficient duration for char formation and porosity without degradation that may occur at longer times. The response Table 7 shows the Signal-to-Noise (S/N) ratios using the "larger is better" criterion identifies the optimal conditions for maximizing the surface area (SA) of biochar. Among the three parameters, pyrolysis temperature has the highest

Table 5
Proximate analysis of the macroalgae *Spirogyra* biomass and biochar.

Sample name	*Proximate analysis (%)			Ultimate analysis (%)				
	VM	ASH	FC	C	H	N	S	O#
Biomass	40.12 ± 0.41	52.24 ± 0.67	7.64 ± 0.39	14.39	1.6	1.16	0.5	30.11
A2	35.73 ± 0.76	59.40 ± 1.20	4.20 ± 0.23	12.64	0.41	0.56	0.17	26.82
A7	29.78 ± 0.47	65.26 ± 0.33	4.96 ± 0.28	13.94	0.65	0.82	0.32	19.01

Table 6
pH results of all 9 set of algal biochar.

Run	Temp-Heating Rate- Residence Time	pH
1	A-450-5-60	9.01
2	A-550-10-90	9.11
3	A-650-15-120	9.72
4	A-450-10-120	8.84
5	A-550-15-60	9.18
6	A-650-5-90	9.51
7	A-450-15-90	8.70
8	A-550-5-120	8.88
9	A-650-10-60	9.80

influence (Delta = 6.15) on SA, followed by heating rate (Delta = 5.79) and residence time (Delta = 4.49).

From Table 7 and the Main Effects Plot Fig. 8 (b) for SA using Signal-to-Noise (S/N) ratios confirm that a pyrolysis temperature of 550 °C, a heating rate of 10 °C/min, and a residence time of 90 min are the most robust settings for maximizing surface area, as these conditions consistently yield higher SA with less variability. Interaction plots further reveal strong interactions, especially between temperature and heating rate, and between heating rate and residence time, highlighting that SA is maximized only when the right combination of parameters is used together. At higher temperatures like 650 °C, increasing the heating rate doesn't improve SA, while higher heating rates (15 °C/min) generally result in poor SA across all residence times and temperatures. These findings emphasize that optimal SA is achieved not only by selecting the best individual values but also by carefully tuning parameter combinations to avoid structural collapse or insufficient pore development.

4.2. Result for O/C

The main effects plot Fig. 9(a) for O/C shows that pyrolysis temperature significantly influences the oxygen-to-carbon ratio, with O/C peaking at 550 °C and dropping sharply at 650 °C, indicating reduced oxygen-containing functional groups due to enhanced carbonization at higher temperatures. The heating rate shows minimal impact, though a slight increase at 10 °C/min suggests improved functionality, making it moderately favorable. Residence time has a notable effect, with O/C lowest at 60 min, peaking at 90 min, and then slightly declining at 120 min, suggesting that 90 min provides optimal conditions for retaining oxygen groups before further degradation occurs.

The analysis of the S/N ratio in Table 8 for the O/C ratio reveals that residence time is the most influential factor (highest delta = 2.412), followed by temperature (delta = 1.932), while heating rate has the least impact (delta = 0.534). The S/N main effects plot in Fig. 9(b) and Table 8 confirms that 550 °C, 10 °C/min, and 90 min are optimal settings for maximizing the O/C ratio, as higher temperatures and faster heating degrade oxygen-containing functional groups. The interaction plots further illustrate how combinations of factors influence O/C; non-

Table 7
SA response table for signal to noise ratios.

Level	T (°C)	Ht (°C/min)	Rt (min)
1	20.71	25.10	23.14
2	26.86	27.31	27.63
3	26.36	21.52	23.16
Delta	6.15	5.79	4.49
Rank	1	2	3

*Larger is better.

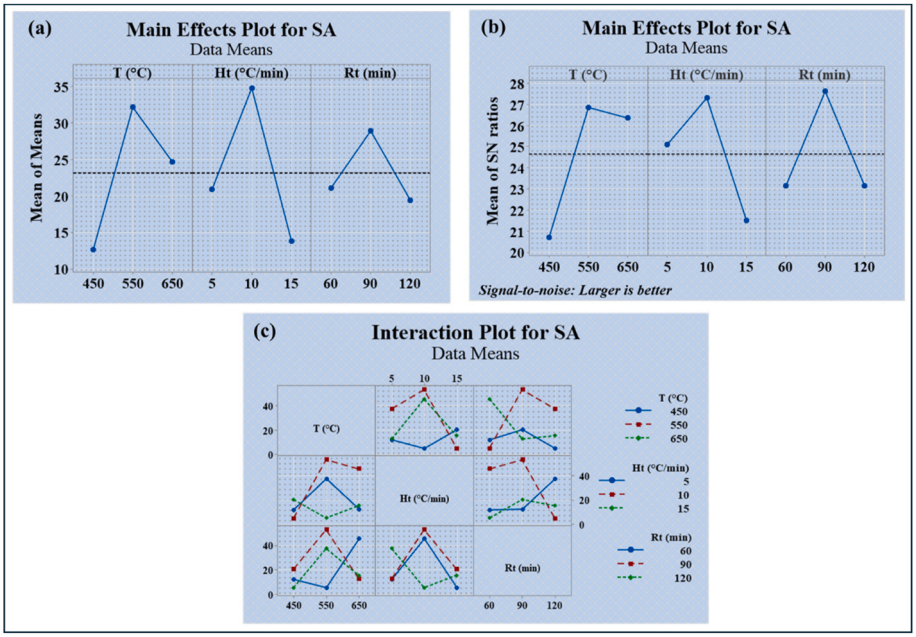

Fig. 8. Main Effect Plot for SA (a) Means of Means (b) S/N ratios and (c) Interaction plot for SA.

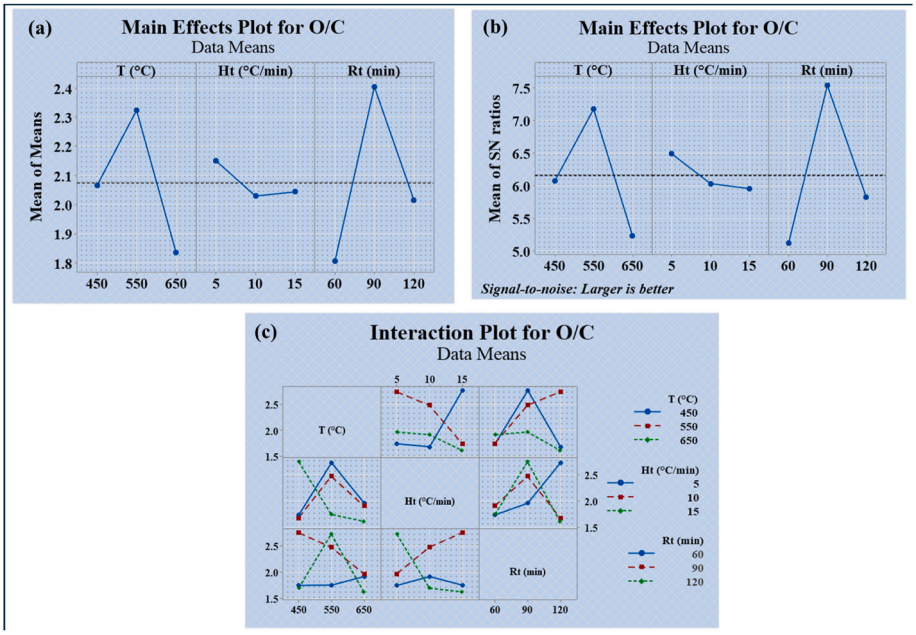

Fig. 9. Main Effect Plot for SA (a) Means of Means (b) S/N ratios and (c) Interaction plot for O/C.

Table 8
O/C response table for signal to noise ratios.

Level	T (°C)	Ht (°C/min)	Rt (min)
1	6.071	6.489	5.118
2	7.168	6.031	7.530
3	5.236	5.954	5.826
Delta	1.932	0.534	2.412
Rank	2	3	1

* Larger is better.

parallel lines (e.g., between temperature and residence time, and heating rate and residence time) indicate strong interactions, where changes in one factor significantly affect the outcome depending on the level of the other. Across interactions, high temperature (650 °C) consistently leads to low O/C values, suggesting excessive carbonization that eliminates oxygen groups. Conversely, a 10 °C/min heating rate synergizes well with both 550 °C and 90 min, while 15 °C/min heating uniformly results in lower O/C ratios, likely due to rapid devolatilization. These plots underscore that moderate temperature and heating rate combined with sufficient residence time are crucial for preserving or enhancing oxygen-containing groups in biochar, with temperature being the most dominant factor in determining final O/C outcomes.

4.3. H/C output

Fig. 10(a) shows the main effects of process parameters on the H/C ratio. It is evident that temperature (T) has a significant impact — as T increases from 450 °C to 650 °C, the H/C ratio sharply decreases,

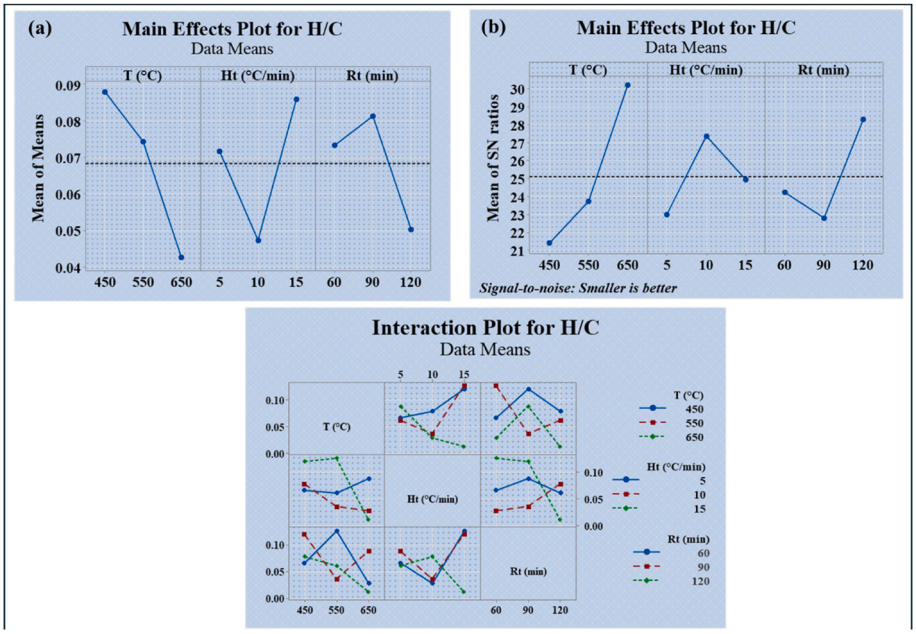

Fig. 10. Main Effect Plot for SA (a) Means of Means (b) S/N ratios and (c) Interaction plot for H/C.

Table 9
H/C response table for signal to noise ratios.

Level	T (°C)	Ht (°C/min)	Rt (min)
1	21.39	23.00	24.22
2	23.72	27.36	22.80
3	30.19	24.94	28.29
Delta	8.80	4.36	5.49
Rank	1	3	2

* Smaller is better.

indicating enhanced aromaticity and thermal maturity of the biochar. Similarly, increasing the heating rate to 10 °C/min initially reduces H/C, but further increasing to 15 °C/min increases it again — suggesting incomplete dehydrogenation at higher rates. For residence time (Rt), 90 min results in the lowest H/C ratio, likely due to sufficient devolatilization and carbon rearrangement. Fig. 10(b), the Main Effects Plot for H/C based on Signal-to-Noise (S/N) ratios under the "Smaller is Better" criterion, shows that temperature has the most significant influence on reducing the H/C ratio, with the highest S/N observed at 650 °C, indicating enhanced carbon stability and aromaticity at this level. The heating rate of 10 °C/min also results in a better (lower) H/C ratio, likely due to more controlled devolatilization, while the residence time of 120 min gives the best outcome among its levels, though its effect is less steep. The S/N response table in Table 9 shows that temperature (T) has the most significant impact ($\Delta = 8.80$, Rank 1) on H/C, followed by residence time (Rt) ($\Delta = 5.49$, Rank 2), and heating rate (Ht) ($\Delta = 4.36$, Rank 3). The interaction plot Fig. 10(c) for the H/C ratio reveals significant interaction effects among temperature, heating rate, and residence time, as indicated by the non-parallel lines. The most prominent interaction is between temperature and heating rate, where the benefit of a high temperature (650 °C) in reducing the H/C ratio is maximized when paired with a lower heating rate (10 °C/min). Additionally, longer residence times (90–120 min) further enhance this effect, leading to consistently low H/C values. These interactions highlight that the influence of one parameter on the H/C ratio is strongly dependent on the levels of the others, confirming that optimal biochar stability is achieved through a synergistic combination of high temperature, slow heating, and sufficient residence time.

4.4. Yield output

The graphical analysis in the provided figure offers valuable insight into the influence of process parameters on the Yield (%). In Fig. 11(a), the Main Effects Plot illustrates how individual parameters temperature (T), heating rate (Ht), and residence time (Rt) affect the mean yield. Yield shows a declining trend with increasing temperature, where 450 °C yields the highest and 650 °C the lowest, indicating that lower temperatures are more favorable for yield. The heating rate shows a slight increase in yield from 5 °C/min to 15 °C/min, suggesting faster heating may enhance yield marginally. Residence time exhibits a peak at 90 min, while both 60- and 120-min results in lower yields, indicating that an optimal hold time is essential.

The response table, Table 10 for signal-to-noise ratios (S/N) using the "Larger is Better" criterion reveals the relative influence of the process parameters Temperature (T), Heating Rate (Ht), and Residence Time (Rt) on maximizing yield. Among the three, temperature has the most significant impact, indicated by the highest delta value of 1.04, suggesting it plays the most critical role in enhancing yield consistency and magnitude. Residence time ranks second (delta = 0.56), while heating rate shows the least influence with a delta of just 0.20. Fig. 11(b), the Main Effects Plot for Signal-to-Noise (S/N) Ratios, supports these observations with a "larger is better" criterion, reinforcing that 450 °C, 15 °C/min, and 90 min are optimal conditions for maximizing consistent yield. Fig. 11(c) presents the Interaction Plot, showing how these parameters interact. Strong interactions are observed between temperature and residence time, where lower temperatures combined with moderate residence time (90 min) yield better results. Interactions between heating rate and other parameters are relatively moderate but still impactful, particularly at extreme values. Overall, the plots collectively indicate that a lower temperature (450 °C), a higher heating rate (15 °C/min), and an intermediate residence time (90 min) are the most effective conditions for maximizing and stabilizing yield.

5. Pearson correlation matrix

In the present study, the Pearson correlation matrix was employed as a complementary statistical tool to the Taguchi optimization framework. While the Taguchi method systematically identified optimal process parameter combinations, the correlation analysis provided additional

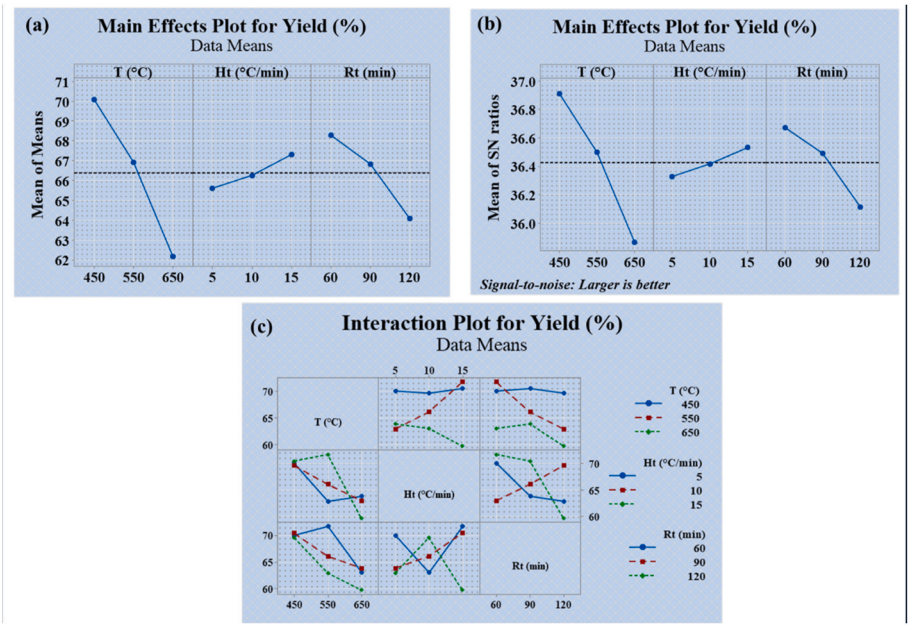

Fig. 11. Main Effect Plot for SA (a) Means of Means (b) S/N ratios and (c) Interaction plot for Yield.

Table 10
Yield response table for signal to noise ratios.

Level	T (°C)	Ht (°C/min)	Rt (min)
1	36.91	36.33	36.67
2	36.50	36.42	36.49
3	35.87	36.53	36.11
Delta	1.04	0.20	0.56
Rank	1	3	2

* Larger is better.

insights into the interrelationships between processing variables (temperature, residence time, heating rate) and biochar properties (yield, H/C, O/C, surface area, particle density). This statistical mapping of relationships informed the material design rationale by revealing which parameters exerted the strongest positive or negative influence on targeted properties, thereby supporting the selection of control factors for optimization. For instance, the observed strong negative correlations between temperature and yield, as well as between heating rate and surface area, validated trends seen in the Taguchi main effect plots and reinforced the mechanistic understanding that higher thermal severity promotes devolatilization, increases surface area, and decreases hydrogen and oxygen content. Although the Pearson correlation results were not used in isolation to set the optimum levels, they served as a cross-validation tool for the Taguchi results and provided a mechanistic justification for the observed trends in biochar formation.

In Fig. 12(A), the Pearson correlation coefficient matrix was generated using five variables with respect to temperature. After running the program, the output parameters, algal biochar yield, H/C, O/C, surface area, and particle density were analyzed for their temperature dependence. The matrix revealed the inter-correlation among these variables, where positive correlations indicated a direct proportionality to temperature. This means that as temperature increased, surface area and particle density also increased. In contrast, the negative correlation of biochar yield, H/C, and O/C ratios with temperature indicates that as temperature increases, these values decrease, showcasing an inverse relationship with temperature. From Fig. 12(B) shows the correlation matrix between residence time and 5 other output variables shows a significant relation between residence time, as it increased, in influenced negatively yield, H/C, and surface area, where it has a positive relation with O/C and particle density. Similarly, from Fig. 12(C) it showed the correlation between heating rate with the same variable parameters, and heating rate has also a significant negative effect on yield, O/C, surface area and particle density, positive correlation with H/C only. From the above Figures Majorly, Temperature, heating rate, and residence time are collectively inversely proportional to algal biochar yield [39,94].

6. Discussion on the effect of processing parameters on biochar properties

The Taguchi analysis of nine pristine algal biochar samples confirmed that pyrolysis temperature, heating rate, and residence time strongly govern yield, functional group composition, and surface area. The same trends were validated by the Pearson correlation matrix, underscoring the robustness of the observed relationships. As shown in Fig. 13, biochar yield decreased markedly with temperature, from 450 °C to 650 °C. This inverse relationship is well documented for both lignocellulosic and algal feedstocks, where higher temperatures promote extensive devolatilization, secondary cracking, and ash formation [41,42]. While yield declined, surface area and functional group development improved with temperature, peaking at 550 °C. This agrees with Keiluweit et al. (2010) [46], who reported that intermediate pyrolysis temperatures balance pore formation with retention of surface oxygen functionality. Heating rate and residence time showed more nuanced effects. A moderate heating rate (10 °C/min) and residence time of 90 min (sample A2) produced the highest BET surface area (53.382 $m^2 g^{-1}$) and O/C ratio (Fig. 14). Moderate heating appears to allow gradual volatile evolution, promoting stable pore structures without collapse—similar to trends observed by Cantrell et al. (2012) [44]. In contrast, the fastest heating rate (15 °C/min) at 450 °C yielded biochar A7 with the highest O/C ratio and abundant oxygenated functional groups, confirmed by FTIR and XPS. Such hydrophilic surfaces favour electrostatic interactions, enhancing metal ion adsorption [94].

Residence time also critically influenced outcomes. Shorter times (60 min) may limit carbonization, while longer durations (120 min) promote gasification losses. The 90-min optimum aligns with Liu et al.

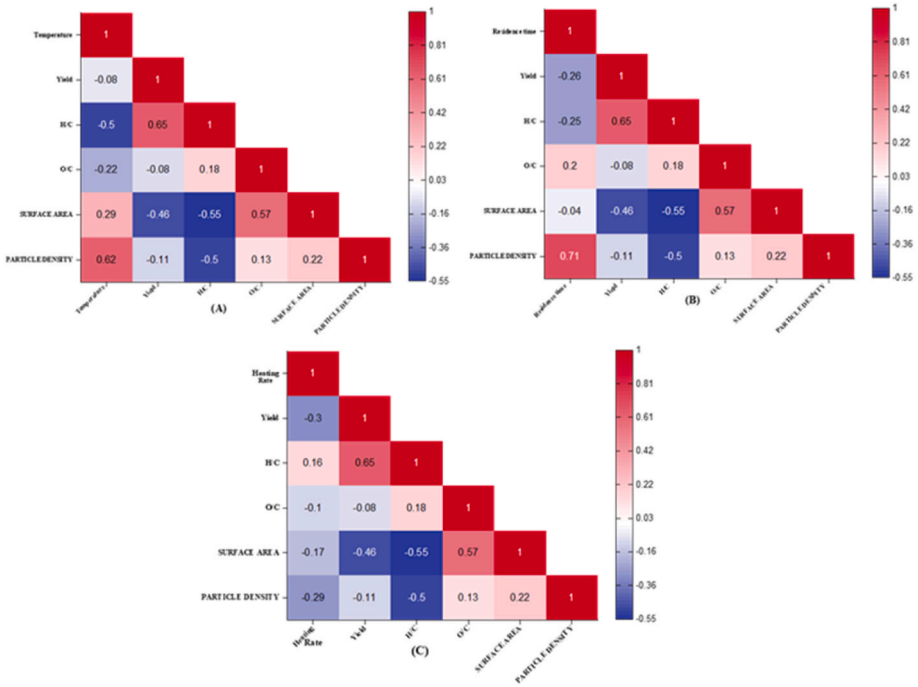

Fig. 12. (A)- Pearson correlation matrix of total of 6 variables with respect to temperature, **(B)**- Residence Time, **(C)**- Heating rate.

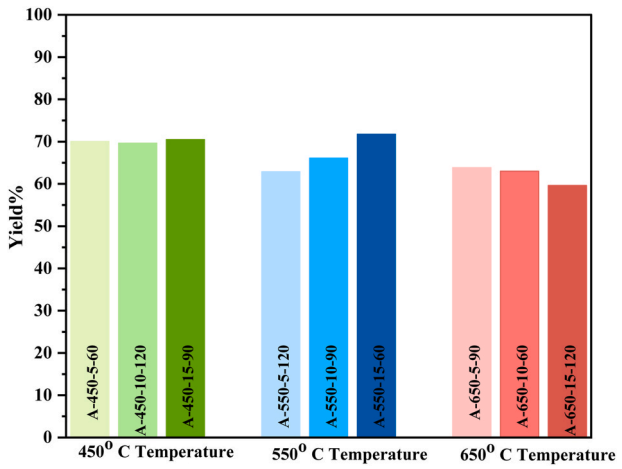

Fig. 13. Bar diagram showing percentage yield of 9 sets of Pristine algal biochar with respect to temperature.

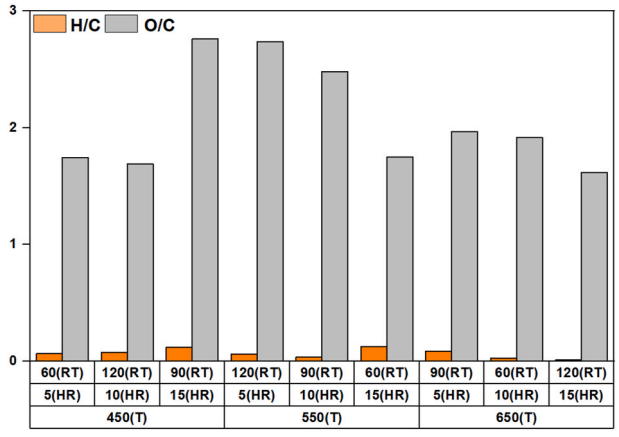

Fig. 14. Bar diagram showing H/C, O/C of 9 sets of Pristine algal biochar with respect to Temperature (T) in °C, Heating rate (HR) in °C/min, Residence Time (RT) in minutes.

(2021) [45], who found that moderate holding times preserved functional groups while enhancing aromaticity. Raman spectra for A2 and A7 revealed pronounced D- and G-bands, indicating aromatic ring structures typical of biochars with high adsorption potential. The feedstock's origin in shrimp-farm algal blooms influenced mineralogy. PXRD, EDS, and proximate analyses revealed high silica and inorganic salt content, likely due to the marine environment. While the fixed carbon content was lower than in lignocellulosic biochars, the mineral-rich composition confers intrinsic ion-exchange capacity and catalytic potential, consistent with findings for other seaweed-derived biochars [95]. Overall, A2 (550 °C, 10 °C/min, 90 min) is optimal for surface-area-driven applications, while A7 (450 °C, 15 °C/min, 90 min) offers superior functional group abundance for electrostatic adsorption and catalysis. These findings reinforce the conclusion that processing parameters must be tailored to the intended end-use, as biochar properties are inherently feedstock- and process-specific [96].

The established relationship provides a novel strategy for evaluating biochars derived from algal blooms (*Spirogyra*) collected from shrimp culture ponds. By optimizing pyrolysis parameters—temperature, heating rate, and residence time—via the Taguchi L9 orthogonal array, biochar quality was enhanced across nine pristine algal biochar sets. Among them, A2 exhibited the highest surface area (53.382 $m^2 g^{-1}$) and a low C/H ratio (0.036), reflecting high aromaticity and structural stability. Such features are advantageous for heavy metal removal, as large surface area and condensed aromatic domains provide abundant sorption sites for Cr (VI), Pb^{2+}, and Cd^{2+} through both physical adsorption and π–π-cation interactions [43,94]. Conversely, A7 achieved the highest yield (70.5 %) with a greater C/O ratio (2.760), a moderate C/H ratio (0.120), and abundant oxygenated functional groups arising from its lower pyrolysis temperature (450 °C). High O-containing groups, coupled with mineral content from the feedstock, enhance ion-exchange and complexation capacity, making A7 suitable for soil amendment to improve nutrient retention, cation exchange capacity, and microbial activity [95,96].

The particle density of both A2 and A7 (1.5–2 g/cm^3) indicates mechanical stability, supporting their use as structural or conductive fillers in composite electrodes for supercapacitors or batteries when hybridised with conductive additives, as demonstrated in algae-derived carbon studies [97,98]. Additionally, the feedstock's natural abundance of silica, Ca, and Mg—confirmed by PXRD and EDS—confers catalytic potential for advanced oxidation and transesterification reactions. By converting nutrient-rich shrimp farm algal blooms, typically a waste product, into application-specific biochars without chemical activation, this approach offers a cost-effective and environmentally sustainable route to multifunctional materials for wastewater remediation, sustainable agriculture, and renewable energy storage.

7. Conclusion

This research employed an innovative integrated approach to assess biochar quality using the Taguchi method and Pearson correlation matrix. The established relationship provides a novel strategy for evaluating biochars derived from algal blooms (Spirogyra) collected from shrimp culture ponds. By optimizing the pyrolysis process through primary parameters, i.e., temperature, heating rate, and residence time, biochar quality was enhanced and validated using the Taguchi L9 orthogonal array, producing 9 sets of pristine algal biochar. Among them, A2 exhibited the highest surface area (53.382 m^2/g) and a C/H ratio of 0.036, indicating higher aromaticity and stability. Meanwhile, A7 demonstrated the highest yield (70.5 %) with a greater C/O ratio of 2.760, a C/H ratio of 0.120, and a higher number of functional groups due to the lower pyrolysis temperature (450 °C). The algal feedstock, sourced from shrimp culture ponds, contributed significantly to biochar composition, being rich in minerals, silica, and inorganic salts but lower in carbon content. The particle density of algal biochar ranged from 1.5 to 2 g/cm^3, aligning with common biochar properties and indicating superior mechanical stability for composite material applications. Due to its rich functional groups, pristine algal biochar holds promise for catalytic reactions, wastewater treatment, pollutant removal, and direct soil amelioration. Since algal blooms from shrimp farms are typically considered waste, this approach is both economical and environmentally friendly, as it requires no chemical treatment. Overall, this methodology establishes a strong foundation for refining and advancing the qualitative and quantitative development of pristine algal biochar.

CRediT authorship contribution statement

Shushree Prachi Palai: Writing – original draft, Visualization, Validation, Software, Resources, Methodology, Investigation, Formal analysis, Data curation. **Soumyaranjan Senapati:** Writing – original draft, Validation, Software, Methodology, Formal analysis, Data curation. **Sthitiprajna Muduli:** Writing – original draft, Visualization, Validation, Software, Methodology, Formal analysis, Data curation. **Alok Kumar Panda:** Validation, Software, Resources, Methodology, Formal analysis, Data curation. **Tapan Kumar Bastia:** Writing – review & editing, Visualization, Supervision, Resources, Methodology, Investigation, Funding acquisition, Conceptualization. **Pankaj Kumar Parhi:** Writing – review & editing, Visualization, Supervision, Resources, Project administration, Investigation, Funding acquisition, Data curation, Conceptualization.

Acknowledgements

All the co-authors are thankfully acknowledged to their host Organizations for providing the necessary facilities to carry out this work. Thanks and acknowledgements to Dr. Sandip Pattanaik, Dr. Puja Priyadarshini Nayak, and Dr. Barada Prasanna Sahoo for providing and extending sincere analytical support during the execution and investigation of this work.

Appendix A. Supplementary data

Supplementary data to this article can be found online at https://doi.org/10.1016/j.biombioe.2025.108401.

Data availability

Data will be made available on request.

References

[1] R. Azargohar, K.L. Jacobson, E.E. Powell, A.K. Dalai, Evaluation of properties of fast pyrolysis products obtained, from Canadian waste biomass, J. Anal. Appl. Pyrolysis 104 (2013) 330–340, https://doi.org/10.1016/j.jaap.2013.06.016.
[2] L.R. Jeeru, F.K. Abdul, J.S. Anireddy, V.P. Ch, K.N. Dhanavath, Optimization of process parameters for conventional pyrolysis of algal biomass into bio–oil and bio–char production, Chemical Engineering and Processing-Process Intensification 185 (2023) 109311, https://doi.org/10.1016/j.cep.2023.109311.
[3] M. Lee, Y.L. Lin, P.T. Chiueh, W. Den, A. Environmental and energy assessment of biomass residues to biochar as fuel: a brief review with recommendations for future bioenergy systems, J. Clean. Prod. 251 (2020) 119714, https://doi.org/10.1016/j.jclepro.2019.119714.
[4] Y.D. Chen, F. Liu, N.Q. Ren, S.H. Ho, Revolutions in algal biochar for different applications: state-of-the-art techniques and future scenarios, Chin. Chem. Lett. 31 (10) (2020) 2591–2602, https://doi.org/10.1016/j.cclet.2020.08.019.
[5] J. Lehmann, J. Gaunt, M. Rondon, Bio-char sequestration in terrestrial ecosystems–a review, Mitig. Adapt. Strategies Glob. Change 11 (2006) 403–427, https://doi.org/10.1007/s11027-005-90065.
[6] D. Mohan, A. Sarswat, Y.S. Ok, C.U. Pittman Jr, Organic and inorganic contaminants removal from water with biochar, a renewable, low cost and sustainable adsorbent–a critical review, Bioresour. Technol. 160 (2014) 191–202, https://doi.org/10.1016/j.biortech.2014.01.120.
[7] M.E. González, M. Cea, D. Reyes, L. Romero-Hermoso, P. Hidalgo, S. Meier, R. Navia, Functionalization of biochar derived from lignocellulosic biomass using microwave technology for catalytic application in biodiesel production, Energy Convers. Manag. 137 (2017) 165–173, https://doi.org/10.1016/j.enconman.2017.01.063.
[8] Y.Y. Wang, H.H. Lu, Y.X. Liu, S.M. Yang, Removal of phosphate from aqueous solution by SiO 2–biochar nanocomposites prepared by pyrolysis of vermiculite treated algal biomass, RSC Adv. 6 (87) (2016) 83534–83546, https://doi.org/10.1039/C6RA15532D.
[9] A.E. Creamer, B. Gao, Carbon-based adsorbents for postcombustion CO2 capture: a critical review, Environ. Sci. Technol. 50 (14) (2016) 7276–7289, https://doi.org/10.1021/acs.est.6b00627.
[10] M.I. Inyang, B. Gao, Y. Yao, Y. Xue, A. Zimmerman, A. Mosa, X. Cao, A review of biochar as a low-cost adsorbent for aqueous heavy metal removal, Crit. Rev. Environ. Sci. Technol. 46 (4) (2016) 406–433, https://doi.org/10.1080/10643389.2015.1096880.
[11] B. Wang, B. Gao, J. Fang, Recent advances in engineered biochar productions and applications, Crit. Rev. Environ. Sci. Technol. 47 (22) (2017) 2158–2207, https://doi.org/10.1080/10643389.2017.1418580.
[12] C. Zhang, L. Liu, M. Zhao, H. Rong, Y. Xu, The environmental characteristics and applications of biochar, Environ. Sci. Pollut. Control Ser. 25 (2018) 21525–21534, https://doi.org/10.1007/s11356-018-2521-1.
[13] S. Dhiman, M. Ibrahim, K. Devi, N. Sharma, N. Kapoor, R. Kaur, R. Bhardwaj, Biochar assisted remediation of toxic metals and metalloids, Handbook of Assisted and Amendment: Enhanced Sustainable Remediation Technology (2021) 131–162, https://doi.org/10.1002/9781119670391.ch7.
[14] K.L. Yu, B.F. Lau, P.L. Show, H.C. Ong, T.C. Ling, W.H. Chen, J.S. Chang, Recent developments on algal biochar production and characterization, Bioresour. Technol. 246 (2017) 2–11, https://doi.org/10.1016/j.biortech.2017.08.009.
[15] M.I. Bird, C.M. Wurster, P.H. de Paula Silva, N.A. Paul, R. De Nys, Algal biochar: effects and applications, GCB Bioenergy 4 (1) (2012) 61–69, https://doi.org/10.1111/j.1757-1707.2011.01109.x.
[16] J. Escalante, W.H. Chen, M. Tabatabaei, A.T. Hoang, E.E. Kwon, K.Y.A. Lin, A. Saravanakumar, Pyrolysis of lignocellulosic, algal, plastic, and other biomass wastes for biofuel production and circular bioeconomy: a review of thermogravimetric analysis (TGA) approach, Renew. Sustain. Energy Rev. 169 (2022) 112914, https://doi.org/10.1016/j.rser.2022.112914.
[17] K. Brindhadevi, S. Anto, E.R. Rene, M. Sekar, T. Mathimani, N.T.L. Chi, A. Pugazhendhi, Effect of reaction temperature on the conversion of algal biomass to bio-oil and biochar through pyrolysis and hydrothermal liquefaction, Fuel 285 (2021) 119106, https://doi.org/10.1016/j.fuel.2020.119106.
[18] C.D. Venkatachalam, S.R. Ravichandran, M. Sengottian, Lignocellulosic and algal biomass for bio-crude production using hydrothermal liquefaction: conversion techniques, mechanism and process conditions: a review, Environ. Eng. Res. 27 (1) (2022) 200555, https://doi.org/10.4491/eer.2020.555, 200550.
[19] R.Y. Krishnan, S. Manikandan, R. Subbaiya, W. Kim, N. Karmegam, M. Govarthanan, Advanced thermochemical conversion of algal biomass to liquid and gaseous biofuels: a comprehensive review of recent advances, Sustain. Energy Technol. Assessments 52 (2022) 102211, https://doi.org/10.1016/j.seta.2022.102211.
[20] S. Das, K. Nath, V.K. Gupta, R. Chowdhury, Studies on power plant algae: assessment of growth kinetics and bio-char production from slow pyrolysis process, Indian Chem. Eng. 63 (2) (2021) 129–138, https://doi.org/10.1080/00194506.2020.1845987.
[21] M.A. Babatabar, F. Yousefian, M.V. Mousavi, M. Hosseini, A. Tavasoli, Pyrolysis of lignocellulosic and algal biomasses in a fixed-bed reactor: a comparative study on the composition and application potential of bioproducts, Int. J. Energy Res. 46 (7) (2022) 9836–9850, https://doi.org/10.1002/er.7855.
[22] S. Pourkarimi, A. Hallajisani, A. Alizadehdakhel, A. Nouralishahi, Biofuel production through micro-and macroalgae pyrolysis–A review of pyrolysis methods and process parameters, J. Anal. Appl. Pyrolysis 142 (2019) 104599, https://doi.org/10.1016/j.jaap.2019.04.015.
[23] P. Choudhary, P.P. Assemany, F. Naaz, A. Bhattacharya, J. de Siqueira Castro, E.D. A. do Couto Couto, A. Malik, A review of biochemical and thermochemical energy conversion routes of wastewater grown algal biomass, Sci. Total Environ. 726 (2020) 137961, https://doi.org/10.1016/j.scitotenv.2020.137961.
[24] S. Tabrett, I. Ramsay, B. Paterson, M.A. Burford, A review of the benefits and limitations of waste nutrient treatment in aquaculture pond facilities, Rev. Aquacult. 16 (4) (2024) 1766–1786, https://doi.org/10.1111/raq.12921.
[25] L.Z. Xia, L.Z. Yang, M.C. Yan, Nitrogen and phosphorus cycling in shrimp ponds and the measures for sustainable management, Environ. Geochem. Health 26 (2) (2004) 245–251, https://doi.org/10.1023/B:EGAH.0000039587.64830.43.
[26] W.A. Wurtsbaugh, H.W. Paerl, W.K. Dodds, Nutrients, eutrophication and harmful algal blooms along the freshwater to marine continuum, Wiley Interdisciplinary Reviews: Water 6 (5) (2019) e1373, https://doi.org/10.1002/wat2.1373.
[27] J. Lan, P. Liu, X. Hu, S. Zhu, Harmful algal blooms in eutrophic marine environments: causes, monitoring, and treatment, Water 16 (17) (2024) 2525, https://doi.org/10.3390/w16172525.
[28] K.M. Poo, E.B. Son, J.S. Chang, X. Ren, Y.J. Choi, K.J. Chae, Biochars derived from wasted marine macro-algae (Saccharina japonica and Sargassum fusiforme) and their potential for heavy metal removal in aqueous solution, J. Environ. Manag. 206 (2018) 364–372, https://doi.org/10.1016/j.jenvman.2017.10.056.
[29] H.J. Cho, K. Baek, J.K. Jeon, S.H. Park, D.J. Suh, Y.K. Park, Removal characteristics of copper by marine macro-algae-derived chars, Chem. Eng. J. 217 (2013) 205–211, https://doi.org/10.1016/j.cej.2012.11.123.
[30] W. Chen, H. Yang, Y. Chen, K. Li, M. Xia, H. Chen, Influence of biochar addition on nitrogen transformation during copyrolysis of algae and lignocellulosic biomass, Environ. Sci. Technol. 52 (16) (2018) 9514–9521, https://doi.org/10.1021/acs.est.8b02485.
[31] R. Gurav, S.K. Bhatia, T.R. Choi, Y.K. Choi, H.J. Kim, H.S. Song, Y.H. Yang, Application of macroalgal biomass derived biochar and bioelectrochemical system with shewanella for the adsorptive removal and biodegradation of toxic azo dye, Chemosphere 264 (2021) 128539, https://doi.org/10.1016/j.chemosphere.2020.128539.
[32] A. Paethanom, K. Yoshikawa, Influence of pyrolysis temperature on rice husk char characteristics and its tar adsorption capability, Energies 5 (12) (2012) 4941–4951, https://doi.org/10.3390/en5124941.
[33] K.W. Jung, T.U. Jeong, H.J. Kang, K.H. Ahn, Characteristics of biochar derived from marine macroalgae and fabrication of granular biochar by entrapment in calcium-alginate beads for phosphate removal from aqueous solution, Bioresour. Technol. 211 (2016) 108–116, https://doi.org/10.1016/j.biortech.2016.03.066.
[34] R. Aniza, W.H. Chen, F.C. Yang, A. Pugazhendh, Y. Singh, Integrating taguchi method and artificial neural network for predicting and maximizing biofuel production via torrefaction and pyrolysis, Bioresour. Technol. 343 (2022) 126140, https://doi.org/10.1016/j.biortech.2021.126140.
[35] N.I. Abd, A.M. Al-Mayah, S.K. Muallah, Microwave pyrolysis of water hyacinth for biochar production using taguchi method, Int. J. Eng. Technol. 7 (2018) 121–126.
[36] G. Asgari, A. Dayari, M. Ghasemi, A. Seid-Mohammadi, V.K. Gupta, S. Agarwal, Efficient fluoride removal by preparation, characterization of pyrolysis bone: mixed level design experiment and taguchi L8 orthogonal array optimization, J. Mol. Liq. 275 (2019) 251–264, https://doi.org/10.1016/j.molliq.2018.10.137.
[37] S.S.A. Syed-Hassan, M.S.M. Zaini, Optimization of the preparation of activated carbon from palm kernel shell for methane adsorption using taguchi orthogonal array design, Kor. J. Chem. Eng. 33 (2016) 2502–2512, https://doi.org/10.1007/s11814-016-0072-z.
[38] Z. Loloie, M. Mozaffarian, M. Soleimani, N. Asassian, Carbonization and CO 2 activation of scrap tires: optimization of specific surface area by the taguchi method, Kor. J. Chem. Eng. 34 (2017) 366–375, https://doi.org/10.1007/s11814-016-0266-4.
[39] R.A.C. Flores, F.P. García, E.M.O. Sánchez, A.M.B. Miró, O.A.A. Sandoval, Pyrolysis optimization of agricultural waste using taguchi L9 orthogonal array design. https://doi.org/10.20944/preprints201712.0087.v1, 2017.
[40] W. Barszcz, M. Łożyńska, J. Molenda, Impact of pyrolysis process conditions on the structure of biochar obtained from Apple waste, Sci. Rep. 14 (1) (2024) 10501, https://doi.org/10.1038/s41598-024-61394-8[.

[41] G. Gascó, J. Paz-Ferreiro, M.L. Álvarez, A. Saa, A. Méndez, Influence of pyrolysis conditions on biochar formation from different feedstocks: a review, Waste Manag. 79 (2018) 335–345, https://doi.org/10.1016/j.wasman.2018.07.042.
[42] L. Zhao, X. Cao, O. Mašek, A. Zimmerman, Roles of pyrolysis temperature in the production of biochar with desirable physicochemical properties for soil amendment, Chemosphere 230 (2019) 329–340, https://doi.org/10.1016/j.chemosphere.2019.05.104.
[43] W. Chen, J. Meng, X. Han, Y. Lan, W. Zhang, Effects of pyrolysis temperature on the yield and physicochemical properties of biochar derived from seaweed, J. Anal. Appl. Pyrolysis 148 (2020) 104853, https://doi.org/10.1016/j.jaap.2020.104853.
[44] K.B. Cantrell, P.G. Hunt, M. Uchimiya, J.M. Novak, K.S. Ro, Impact of pyrolysis temperature and manure source on physicochemical characteristics of biochar, Bioresour. Technol. 107 (2012) 419–428, https://doi.org/10.1016/j.biortech.2011.11.084.
[45] Z. Liu, X. Ma, Y. Zhang, W. Lu, J. Wang, L. Chen, Effects of residence time and temperature on the characteristics of algae-derived biochar, Renew. Energy 168 (2021) 587–596, https://doi.org/10.1016/j.renene.2020.12.060.
[46] M. Keiluweit, P.S. Nico, M.G. Johnson, M. Kleber, Dynamic molecular structure of plant biomass-derived black carbon (biochar), Environ. Sci. Technol. 44 (4) (2010) 1247–1253, https://doi.org/10.1021/es9031419.
[47] S.P. Palai, B.P. Sahoo, S. Senapati, A.K. Panda, T.K. Bastia, P. Rath, P.K. Parhi, A review on exploring pyrolysis potential of invasive aquatic plants, J. Environ. Manag. 371 (2024) 123017, https://doi.org/10.1016/j.jenvman.2024.123017.
[48] W. Lian, L. Yang, S. Joseph, W. Shi, R. Bian, J. Zheng, G. Pan, Utilization of biochar produced from invasive plant species to efficiently adsorb Cd (II) and Pb (II), Bioresour. Technol. 317 (2020) 124011, https://doi.org/10.1016/j.biortech.2020.124011.
[49] O. Farobie, A. Amrullah, N.A. Sholeha, W. Fatriasari, E. Hartulistiyoso, Eco-innovation in energy: solid degradation kinetics of rejected red macroalgae (*kappaphycopsiscottonii*) for bio-oil and biochar production, Results Eng. 22 (2024) 102203, https://doi.org/10.1016/j.rineng.2024.102203.
[50] G. Belotti, B. de Caprariis, P. De Filippis, M. Scarsella, N. Verdone, Effect of Chlorella vulgaris growing conditions on bio-oil production via fast pyrolysis, Biomass Bioenergy 61 (2014) 187–195, https://doi.org/10.1016/j.biombioe.2013.12.011.
[51] C. Xia, A. Pathy, B. Paramasivan, P. Ganeshan, K. Dhamodharan, A. Juneja, K. Rajendran, Comparative study of pyrolysis and hydrothermal liquefaction of microalgal species: analysis of product yields with reaction temperature, Fuel 311 (2022) 121932, https://doi.org/10.1016/j.fuel.2021.121932.
[52] K. Chaiwong, T. Kiatsiriroat, N. Vorayos, C. Thararax, Biochar production from freshwater algae by slow pyrolysis, Maejo International Journal of Science and Technology 6 (2) (2012) 186. https://www.proquest.com/scholarly-journals/biochar-production-freshwater-algae-slow/docview/1081168587/se-2?accountid=151027.
[53] K. Jindo, H. Mizumoto, Y. Sawada, M.A. Sanchez-Monedero, T. Sonoki, Physical and chemical characterization of biochars derived from different agricultural residues, Biogeosciences 11 (23) (2014) 6613–6621, https://doi.org/10.5194/bg-11-6613-2014.
[54] G.A.N. Rohman, M.A. Aziz, A. Nawaz, M.A. Elgzoly, M.M. Hossain, S.A. Razzak, High-performance biochar from Chlorella pyrenoidosa algal biomass for heavy metals removal in wastewater, Sep. Purif. Technol. 341 (2024) 126870, https://doi.org/10.1016/j.seppur.2024.126870.
[55] V. Vasudev, X. Ku, J. Lin, Combustion behavior of algal biochars obtained at different pyrolysis heating rates, ACS Omega 6 (29) (2021) 19144–19152, https://doi.org/10.1021/acsomega.1c02493.
[56] M. Tsarpali, J.N. Kuhn, G.P. Philippidis, Activated carbon production from algal biochar: chemical activation and feasibility analysis, Fuel Communications 19 (2024) 100115, https://doi.org/10.1016/j.jfueco.2024.100115.
[57] J.H. Choi, S.S. Kim, D.J. Suh, E.J. Jang, K.I. Min, H.C. Woo, Characterization of the bio-oil and bio-char produced by fixed bed pyrolysis of the brown alga Saccharina japonica, Kor. J. Chem. Eng. 33 (2016) 2691–2698, https://doi.org/10.1007/s11814-016-0131-5.
[58] D.A. Roberts, N.A. Paul, S.A. Dworjanyn, M.I. Bird, R. de Nys, Biochar from commercially cultivated seaweed for soil amelioration, Sci. Rep. 5 (1) (2015) 9665, https://doi.org/10.1038/srep09665.
[59] N. Bordoloi, R. Narzari, D. Sut, R. Saikia, Characterization of bio-oil and its sub-fractions from pyrolysis of *Scenedesmus dimorphus*, Renew. Energy 98 (4) (2016) 245–253, https://doi.org/10.1016/j.renene.2016.03.081.
[60] F. Ronsse, S. Van Hecke, D. Dickinson, W. Prins, Production and characterization of slow pyrolysis biochar: influence of feedstock type and pyrolysis conditions, GCB Bioenergy 5 (2) (2013) 104–115, https://doi.org/10.1111/gcbb.12018.
[61] T. Pak, K.E. Gomari, S. Bose, T. Tonon, D. Hughes, M. Gronnow, D. Macquarrie, Biochar from brown algae: production, activation, and characterisation, Bioresour. Technol. Rep. 24 (2023) 101688, https://doi.org/10.1016/j.biteb.2023.101688.
[62] A. Rekha, L. Srinivasan, S. Pavithra, T. Gomathi, P.N. Sudha, G. Lavanya, A. Vidhya, Biosorption efficacy studies of Sargassum wightii and its biochar on the removal of chromium from aqueous solution, J. Taiwan Inst. Chem. Eng. 166 (2025) 105241, https://doi.org/10.1016/j.jtice.2023.105241.
[63] B. Wang, B. Gao, J. Fang, Recent advances in engineered biochar productions and applications, Crit. Rev. Environ. Sci. Technol. 47 (22) (2017) 2158–2207, https://doi.org/10.1080/10643389.2017.1418580.
[64] J. Jiang, Y. Nie, Fozia, J. Lin, Z. Dai, X. Xu, H. Xu, Preparation of Spirogyra-derived biochar modified electrode and its application in nitrite detection, Biomass Conversion and Biorefinery 14 (14) (2024) 16657–16672, https://doi.org/10.1007/s13399-023-03801-0.
[65] C. Guo, J. Zou, J. Yang, K. Wang, S. Song, Surface characterization of maize-straw-derived biochar and their sorption mechanism for Pb2+ and methylene blue, PLoS One 15 (8) (2020) e0238105, https://doi.org/10.1371/journal.pone.0238105.
[66] M.S. Reza, S. Afroze, M.S. Bakar, R. Saidur, N. Aslfattahi, J. Taweekun, A.K. Azad, Biochar characterization of invasive Pennisetum purpureum grass: effect of pyrolysis temperature, Biochar 2 (2020) 239–251, https://doi.org/10.1007/s42773-020-00048-0.
[67] S. Senapati, J. Giri, L. Mallick, P. Biswal, S. Mohapatra, D. Behera, A.K. Panda, Ultra-fast adsorption of the industrial cationic dye pollutant using nitric acid-activated rice straw biochar: insights into adsorption mechanisms, Biomass Conversion and Biorefinery (2025) 1–19, https://doi.org/10.1007/s13399-025-06540-6.
[68] S. Chauhan, P.A. Taksal, S. Chowdhury, J. Bhattacharya, B.K. Dubey, Unveiling biochar quality index: a factor analysis mediated ranking approach to select best ranked biochar for adsorptive removal of sulfamethoxazole, Ind. Eng. Chem. Res. 63 (27) (2024) 12126–12144, https://doi.org/10.1021/acs.iecr.4c00824.
[69] A. Samanta, D.K. Chanda, P.S. Das, J. Ghosh, A. Dey, S. Das, A.K. Mukhopadhyay, Synthesis of mixed calcite–calcium oxide nanojasmine flowers, Ceram. Int. 42 (2) (2016) 2339–2348, https://doi.org/10.1016/j.ceramint.2015.10.030.
[70] O. Farobie, A. Amrullah, A. Bayu, N. Syaftika, L.A. Anis, E. Hartulistiyoso, In-depth study of bio-oil and biochar production from macroalgae sargassum sp. via slow pyrolysis, RSC Adv. 12 (16) (2022) 9567–9578, https://doi.org/10.1039/D2RA00702A.
[71] S. Senapati, J. Giri, L. Mallick, D. Singha, T.K. Bastia, P. Rath, A.K. Panda, Rapid adsorption of industrial cationic dye pollutant using base-activated rice straw biochar: performance, isotherm, kinetic and thermodynamic evaluation, Discover Sustainability 6 (1) (2025) 46, https://doi.org/10.1007/s43621-025-00835-4.
[72] X. Liu, J. Liao, H. Song, Y. Yang, C. Guan, Z. Zhang, A biochar-based route for environmentally friendly controlled release of nitrogen: urea-loaded biochar and bentonite composite, Sci. Rep. 9 (1) (2019) 9548, https://doi.org/10.1038/s41598-019-46065-3.
[73] X. Li, J.I. Hayashi, C.Z. Li, FT-Raman spectroscopic study of the evolution of char structure during the pyrolysis of a Victorian brown coal, Fuel 85 (12–13) (2006) 1700–1707, https://doi.org/10.1016/j.fuel.2006.03.008.
[74] B. Huang, D. Huang, Q. Zheng, C. Yan, J. Feng, H. Gao, Y. Liao, Enhanced adsorption capacity of tetracycline on porous graphitic biochar with an ultra-large surface area, RSC Adv. 13 (15) (2023) 10397–10407, https://doi.org/10.1039/D3RA00745F.
[75] M. González-Hourcade, G.S. dos Reis, A. Grimm, E.C. Lima, S.H. Larsson, F. G. Gentili, Microalgae biomass as a sustainable precursor to produce nitrogen-doped biochar for efficient removal of emerging pollutants from aqueous media, J. Clean. Prod. 348 (2022) 131280, https://doi.org/10.1016/j.jclepro.2022.131280.
[76] N.S. Kumar, H.M. Shaikh, M. Asif, E.H. Al-Ghurabi, Engineered biochar from wood apple shell waste for high-efficient removal of toxic phenolic compounds in wastewater, Sci. Rep. 11 (1) (2021) 2586, https://doi.org/10.1038/s41598-021-82277-2.
[77] A.M. Golsheikh, H.N. Lim, R. Zakaria, N.M. Huang, Sonochemical synthesis of reduced graphene oxide uniformly decorated with hierarchical ZnS nanospheres and its enhanced photocatalytic activities, RSC Adv. 5 (17) (2015) 12726–12735, https://doi.org/10.1039/C4RA14775H.
[78] Y. Li, S. Li, Y. Wang, J. Wang, H. Liu, X. Liu, N. Ma, Electrochemical synthesis of phosphorus-doped graphene quantum dots for free radical scavenging, Phys. Chem. Chem. Phys. 19 (18) (2017) 11631–11638, https://doi.org/10.1039/C6CP06377B.
[79] H.O. Chahinez, O. Abdelkader, Y. Leila, H.N. Tran, One-stage preparation of palm petiole-derived biochar: characterization and application for adsorption of crystal violet dye in water, Environ. Technol. Innov. 19 (2020) 100872, https://doi.org/10.1016/j.eti.2020.100872.
[80] M. Meng, H. Yan, Y. Jiao, A. Wu, X. Zhang, R. Wang, C. Tian, A "1-methylimidazole-fixation" route to anchor small-sized nitrides on carbon supports as non-Pt catalysts for the hydrogen evolution reaction, RSC Adv. 6 (35) (2016) 29303–29307, https://doi.org/10.1039/C5RA27490G.
[81] O. Auciello, J.F. Veyan, M.J. Arellano-Jimenez, Comparative X-ray photoelectron spectroscopy analysis of nitrogen atoms implanted in graphite and diamond, Frontiers in Carbon 2 (2023) 1279356, https://doi.org/10.3389/frcrb.2023.1279356.
[82] M. Smith, L. Scudiero, J. Espinal, J.S. McEwen, M. Garcia-Perez, Improving the deconvolution and interpretation of XPS spectra from chars by ab initio calculations, Carbon 110 (2016) 155–171, https://doi.org/10.1016/j.carbon.2016.09.012.
[83] T. Ghosh, T. Elo, V.S. Parihar, P. Maiti, R. Layek, Poly (itaconic acid) functionalized lignin/polyvinyl acetate composite resin with improved sustainability and wood adhesion strength, Ind. Crop. Prod. 187 (2022) 115299, https://doi.org/10.1016/j.indcrop.2022.115299.
[84] G. Simoes dos Reis, C. Mayandi Subramaniyam, A.D. Cárdenas, S.H. Larsson, M. Thyrel, U. Lassi, F. Garcia-Alvarado, Facile synthesis of sustainable activated biochars with different pore structures as efficient additive-carbon-free anodes for lithium-and sodium-ion batteries, ACS Omega 7 (46) (2022) 42570–42581, https://doi.org/10.1021/acsomega.2c06054.
[85] Q. Fan, J. Sun, L. Chu, L. Cui, G. Quan, J. Yan, M. Iqbal, Effects of chemical oxidation on surface oxygen-containing functional groups and adsorption behavior of biochar, Chemosphere 207 (2018) 33–40, https://doi.org/10.1016/j.chemosphere.2018.05.044.
[86] Y. Xu, Y. Liu, S. Liu, X. Tan, G. Zeng, W. Zeng, B. Zheng, Enhanced adsorption of methylene blue by citric acid modification of biochar derived from water hyacinth

(Eichornia crassipes), Environ. Sci. Pollut. Control Ser. 23 (2016) 23606–23618, https://doi.org/10.1007/s11356-016-7572-6.
[87] Q. Hu, H. Yang, D. Yao, D. Zhu, X. Wang, J. Shao, H. Chen, The densification of biochar: effect of pyrolysis temperature on the qualities of pellets, Bioresour. Technol. 200 (2016) 521–527, https://doi.org/10.1016/j.biortech.2015.10.077.
[88] X. Gao, C.A. Masiello, 12 analysis of biochar porosity by pycnometry, Biochar: A Guide to Analytical Methods 132 (2017).
[89] K. Weber, P. Quicker, Properties of biochar, Fuel 217 (2018) 240–261, https://doi.org/10.1016/j.fuel.2017.12.054.
[90] J.H. Choi, S.S. Kim, D.J. Suh, E.J. Jang, K.I. Min, H.C. Woo, Characterization of the bio-oil and bio-char produced by fixed bed pyrolysis of the brown alga Saccharina japonica, Kor. J. Chem. Eng. 33 (2016) 2691–2698, https://doi.org/10.1007/s11814-016-0131-5.
[91] F. Ronsse, S. Van Hecke, D. Dickinson, W. Prins, Production and characterization of slow pyrolysis biochar: influence of feedstock type and pyrolysis conditions, GCB Bioenergy 5 (2) (2013) 104–115, https://doi.org/10.1111/gcbb.12018.
[92] A.T. Tag, G. Duman, S. Ucar, J. Yanik, Effects of feedstock type and pyrolysis temperature on potential applications of biochar, J. Anal. Appl. Pyrolysis 120 (2016) 200–206, https://doi.org/10.1016/j.jaap.2016.05.006.
[93] A. Singh, R. Sharma, D. Pant, P. Malaviya, Engineered algal biochar for contaminant remediation and electrochemical applications, Sci. Total Environ. 774 (2021) 145676, https://doi.org/10.1016/j.scitotenv.2021.145676.
[94] M. Inyang, E. Dickenson, M. Peacock, X. Cao, Biochar from anaerobically digested sugarcane bagasse, Bioresour. Technol. 101 (14) (2012) 5220–5228, https://doi.org/10.1016/j.biortech.2012.02.033.
[95] D.A. Roberts, A.J. Cole, A. Whelan, R. de Nys, N.A. Paul, Seaweed-derived biochar for nutrient recovery, J. Appl. Phycol. 27 (5) (2015) 2061–2070, https://doi.org/10.1007/s10811-014-0491-0.
[96] J. Lehmann, S. Joseph, Biochar for Environmental Management: Science, Technology and Implementation, second ed., Routledge, 2015 https://doi.org/10.4324/9780203762264.
[97] A. Boonpoke, S. Chiarakorn, N. Laosiripojana, S. Towprayoon, A. Chidthaisong, N. Worasuwannarak, Preparation of activated carbons from algal biomass for electrochemical energy storage, Carbon 49 (10) (2011) 3259–3267, https://doi.org/10.1016/j.carbon.2011.04.021.
[98] Y. Zhang, X. Ma, J. Yang, Z. Liu, W. Lu, Hierarchical porous carbon derived from algae for high-performance supercapacitors, ACS Sustain. Chem. Eng. 7 (13) (2019) 11440–11449, https://doi.org/10.1021/acssuschemeng.9b01878.